Research Paper

Investigation on Dynamic Response of Sandwich Micro-Beam with Piezo-Electric and Porous Graphene Face-Sheets and Piezo–Magnetic Core Rested on Silica Aerogel Foundation

A. Ghorbanpour Arani [*], P. Pourmousa, E. Haghparast, S. Niknejad

Faculty of Mechanical Engineering, University of Kashan, Kashan, Iran

ABSTRACT

In this study, dynamic response of sandwich micro beam with piezo-electric and porous graphene face sheets and piezo-magnetic core subjected to the electro-magneto-thermal loads is investigated. Silica aerogel foundation is considered as an elastic medium. Modified strain gradient theory (MSGT) is utilized to consider the size effect. Utilizing Hamilton's principle and zigzag deformation beam theory. equations of motion for simply-supported microbeam are derived and solved by Fourier series-Laplace transform method. The effects of various parameters such as small scale, core to face sheets ratio, temperature changes, electric fields intensity and elastic foundation on the transient response of sandwich micro-beam are investigated. As the novelty of the presented work, it should be noted that both piezo-electric and piezo-magnet layers are considered as the sensor; the micro beam is simultaneously subjected to the magnetic, electric, thermal, and mechanical loading; and the foundation is modeled based on the silica aerogel foundation model.

Keywords: Thermal loads; Porous graphene; Piezo-magnetic; Piezo-electric; Silica Aerogel.

1 INTRODUCTION

OVER the last few decades, sandwich structures widely use in the military, aircraft, space station, and industrial. Due to the smart ceramics utilized in the presented work, the sensor of the wind turbines, MAP sensor in the fuel injection in of cars, sonar system in the submarines, smart structures in civil engineering, accelerometer, and military industries can be stated as the practical applications of the present study. Many studies have been done on

_____
[*]Corresponding author. Tel.: +98 31 55912450, Fax: +98 31 55912424.
E-mail address: aghorban@kashanu.ac.ir
.

the dynamic stability of sandwich beams for many years due to the importance of this issue [1-3]. Piezoelectric materials employ in the manufacture of sensors, heat exchanger and medical equipment [4-6]. Li et al. [7] presented the nonlinear dynamic response of beams subjected to the thermal and blast loads. They showed the sine pulse, vibration frequency and amplitude of the nonlinear dynamic responses of beam depend on the periodic excitation. For example, the temperature and axial velocity have an influence on the vibration frequency and flexural amplitude. Ansari et al. [8] studied the dynamic stability of multi-walled carbon nanotubes under the axial compressive load in thermal environment. Using the nonlocal and Timoshenko beam theories on winkler elastic foundation. Kolahchi et al. [9] investigated the thermal and dynamic stability of functionally graded (FG) viscoelastic plates which is resting on orthotropic Pasternak foundation. They considered the distributions of carbon nanotubes in plate as UD, FG-X, FG-O and FG-A and according to the Kelvin–Voigt theory [10] they obtained the material properties of FG viscoelastic plates depend on the time. Shujairi and mollamahmutoglu [11] analyzed the thermal dynamic stability of FG sandwich micro beam by using modified strain gradient theory (MSGT). They observed the material length scale parameter and the nonlocal parameter have the softening effect on stiffness. Ke and Wang [12] analyzed the dynamic stability of FG microbeams by using modified couple stress theory (MCST). Mohammadimehr et al. [13] presented the dynamic stability of viscoelastic piezoelectric plate reinforced by FG carbon nanotubes under thermal, electrical, magnetic and mechanical loadings. They showed that increasing foundation damping coefficient leads to increase the dynamic stability. Tagarielli et al. [14] calculated the dynamic response of glass fibre–vinylester composite beams by impacting the beams at mid-span with metal foam projectiles. By using high-speed photography, they measured the transient transverse deflection of the beams and to record the dynamic modes of deformation and failure. In the next work, they investigated the dynamic shock response of fully clamped monolithic and sandwich beams, with elastic face sheets and a compressible elastic–plastic core [15]. Mohammadimehr et al. [16] considered dynamic stability of carbon nanotubes reinforced composite circular micro sandwich plate based on MSGT. Sahmani and Bahrami [17] analyzed the dynamic stability of micro beams by applying piezoelectric voltage based on MSGT. By using Hamilton's principle, they derived the higher-order governing differential equations and associated boundary conditions. Loja [18] presented dynamic response of soft core sandwich beams with metal-graphene nanocomposite skins. He simulated the viscoelastic behavior of the sandwich core by complex method and solved the dynamic problem by frequency domain. Bhardwaj et al. [19] studied the non-linear flexural and dynamic response of CNT reinforced laminated composite plates. They utilized Halpin–Tsai model to predict the properties of matrix by dispersing CNT in it. Talimian and Beda [20] presented the dynamic stability of micro-beam with simply supports boundary conditions based on MCST. They derived the linear equations of motion by Timoshenko micro beam model. Zamanzadeh et al. [21] studied the dynamic stability of FG micro beam in thermal environment based on classical theory (CT) and MCST. Gao et al. [22] investigated the nonlinear dynamic stability of composite orthotropic plate on Pasternak foundation under thermal load. They showed when temperature increases, it leads to increase the axial compression stresses and reduce the transverse stiffness of composite orthotropic plate. Songsuwan et al. [23] studied free and forced vibration of FG sandwich beams using Timoshenko beam theory under different dynamic loadings. They obtained the equations of motion using Lagrange's equations and selected the Ritz and Newmark models as solution methods. Ojha and Dwivedy [24] presented the dynamic analysis of a sandwich plate with composite layers and viscoelastic core. They obtained the natural frequencies and loss factors of the system by finding the eigenvalues of the dynamic matrix.

With attention to literature review, transient analysis of simply-supported sandwich micro beam with piezo-magnetic core and piezo-electric and porous graphene facesheets subjected to the electro-magneto-thermal loads is a new research which is presented for the first time. The governing equations of motion are derived using Hamilton's principle and MSGT. The analytical approach is proposed for a simply supported micro beam to investigate the influence of different parameters of this issue. The outcomes of this paper can be useful to automotive, aerospace and control of micro- piezomagnetic and piezoelectric devices. As the novelty of this paper, it can be stated that both piezo-magnet and piezo-electric layers are considered as the sensor; the micro beam is simultaneously subjected to the electric, magnetic, mechanical, and thermal loading; and the foundation is modeled based on the silica aerogel foundation model.

2   SANDWICH MICRO-BEAM MODELING

Consider a sandwich micro beam with length L under the electric and magnetic field rested on Silica Aerogel foundation as shown in Fig.1. Also, the thickness of piezo-magnet, piezo-electric, porous graphene layers and Silica Aerogel foundation are h_m, h_e, h_g and H, respectively.
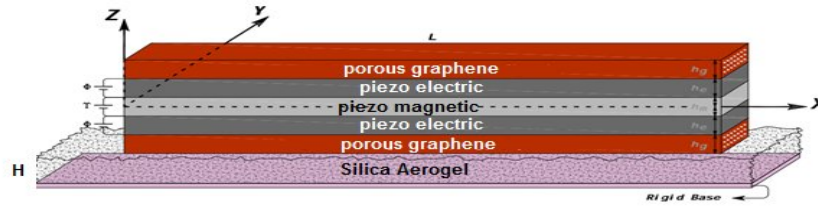
Fig. 1
Sandwich micro beam with piezomagnetic core and piezoelectric and porous graphene facesheet rested on Silica Aerogel Foundation.

According to the zigzag deformation beam theory, the displacement field of sandwich micro beam can be expressed as follows [25]:

$$u_x^k(x,z) = u(x) + z\theta(x) + \varphi^k(z)\psi(x), \tag{1}$$

$$u_x^k(x,z) = w(x), \tag{2}$$

where u and w are the axial and transverse displacement of beam, respectively. Also, $\theta(x)$ is the average bending rotation and $\psi(x)$ is called the amplitude of the zigzag displacement. Note that Superscript k is related to the layers of sandwich beam. The zigzag function $\varphi^k(z)$ can be expressed as follows [26]:

$$\varphi^k(z) = (z+h)\left(\frac{G_s}{Q_{44}^k} - 1\right) \qquad k = 1, \tag{3}$$

$$\varphi^k(z) = (z+h)\left(\frac{G_s}{Q_{44}^k} - 1\right) + \sum_{i=2}^{k}\left(\frac{G_1}{Q_{44}^{i-1}} - \frac{G_1}{Q_{44}^k}\right); \qquad k = 2,3,... \tag{4}$$

The normal strain of five layers of sandwich beam can be expressed as the following relations [27]:

$$\varepsilon_x = \frac{\partial U}{\partial x} = \frac{\partial u(x)}{\partial x} + z\frac{\partial \theta(x)}{\partial x} + \varphi^k(z)\frac{\partial \psi(x)}{\partial x}, \tag{5}$$

$$\gamma_{xz} = \frac{\partial W}{\partial x} + \frac{\partial U}{\partial z} = \frac{\partial W(x)}{\partial x} + \theta(x) + \frac{\partial \varphi^k(z)}{\partial z}\psi(x), \tag{6}$$

where ε_x and γ_{xz} are the normal and shear strains.

2.1 Piezomagnetic core

Stress-strain and magnetic field relations of piezomagnetic core can be defined as follows [28]:

$$
\begin{bmatrix} \sigma_{xx} \\ \sigma_{xz} \end{bmatrix}^m = \begin{bmatrix} Q_{11} & 0 \\ 0 & Q_{55} \end{bmatrix} \begin{bmatrix} \varepsilon_x \\ \gamma_{xz} \end{bmatrix}^m + \begin{bmatrix} 0 & f_{31} \\ f_{15} & 0 \end{bmatrix} \begin{bmatrix} H_x \\ H_z \end{bmatrix},
\tag{7}
$$

$$
\begin{bmatrix} B_x \\ B_z \end{bmatrix} = \begin{bmatrix} f_{15} & 0 \\ 0 & f_{31} \end{bmatrix} \begin{bmatrix} \varepsilon_x \\ \gamma_{xz} \end{bmatrix}^m - \begin{bmatrix} \mu_{11} & 0 \\ 0 & \mu_{33} \end{bmatrix} \begin{bmatrix} H_x \\ H_z \end{bmatrix},
\tag{8}
$$

in which σ and Q indicate stress components and elastic constants and B, H, f and μ are the magnetic inductions, magnetic potential, piezomagnetic constants and magnetic permeability coefficients, respectively.
The distribution of magnetic potential in thickness direction of piezomagnetic core which satisfies the Maxwell's relations can be written as [29]:

$$
\alpha(x,z,t) = -\cos\left(\frac{\pi z}{h_m}\right)\alpha(x,t) + \frac{2z}{h_m}\Omega e^{i\omega t},
\tag{9}
$$

in which, Ω is the initial external magnetic potential applied to the piezomagnetic core. According to Eq. (9), the nonzero components of magnetic fields (H_x and H_z) can be given by [29]:

$$
H_x = -\frac{\partial \alpha}{\partial x} = \cos\left(\frac{\pi z}{h_m}\right)\frac{\partial \alpha}{\partial x},
\tag{10a}
$$

$$
H_z = -\frac{\partial \alpha}{\partial z} = -\frac{\pi}{h_m}\sin\left(\frac{\pi z}{h_m}\right)\alpha + \frac{2}{h_m}\Omega e^{i\omega t}.
\tag{10b}
$$

2.2 Piezoelectric layers

The constitutive equations of piezoelectric layers under electric field can be given by [30]:

$$
\begin{bmatrix} \sigma_{xx} \\ \sigma_{xz} \end{bmatrix}^e = \begin{bmatrix} Q_{11} & 0 \\ 0 & Q_{55} \end{bmatrix} \begin{bmatrix} \varepsilon_x \\ \gamma_{xz} \end{bmatrix}^e + \begin{bmatrix} 0 & e_{31} \\ e_{15} & 0 \end{bmatrix} \begin{bmatrix} E_x \\ E_z \end{bmatrix},
\tag{11}
$$

$$
\begin{bmatrix} D_x \\ D_z \end{bmatrix} = \begin{bmatrix} e_{15} & 0 \\ 0 & e_{31} \end{bmatrix} \begin{bmatrix} \varepsilon_x \\ \gamma_{xz} \end{bmatrix}^e - \begin{bmatrix} h_{11} & 0 \\ 0 & h_{33} \end{bmatrix} \begin{bmatrix} E_x \\ E_z \end{bmatrix},
\tag{12}
$$

in which D, E, e and $\in$ are the electric inductions, electric potential, piezoelectric constants and electric permeability coefficients.
  Different distribution pattern of the electric potential along the thickness direction can be found in the various papers which all of the satisfy the Maxwell's relations in the quasi-static approximation [31-36]. In this paper, the distribution of electric potential along the thickness direction is supposed to be changed as a combination of a cosine as follows [37]:

$$\beta(x,z,t) = \begin{cases} \left[-\cos\left[\dfrac{\pi}{h_e}\left(z-\dfrac{h_m}{2}\right)\right]\right]\beta(x,t)+\dfrac{2}{h_e}\left(z-\dfrac{h_m}{2}\right)V_0\,e^{i\omega t} & \dfrac{h_m}{2}<z<\dfrac{h_m}{2}+h_e \\[4mm] \left[-\cos\left[\dfrac{\pi}{h_e}\left(-z-\dfrac{h_m}{2}\right)\right]\right]\beta(x,t)+\dfrac{2}{h_e}\left(-z-\dfrac{h_m}{2}\right)V_0\,e^{i\omega t} & -\dfrac{h_m}{2}-h_e<z<-\dfrac{h_m}{2} \end{cases} , \tag{13}$$
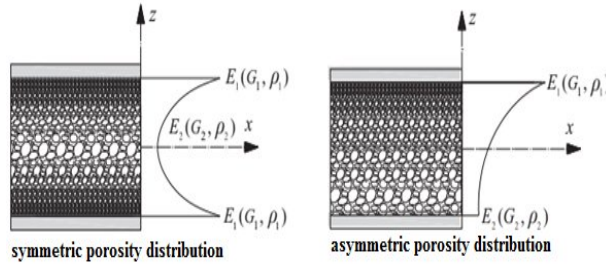
Fig. 2
FG Porous with different porosity distributions [39].

In Eq. (13), ω and V_0 are the natural frequency of system and the initial external electric voltage, respectively. Therefore, the nonzero components of electric fields (E_x and E_z) can be written as [38]:

$$E_x = -\frac{\partial \beta}{\partial x} = \cos\left[\frac{\pi}{h_e}\left(z-\frac{h_m}{2}\right)\right]\frac{\partial \beta}{\partial x}, \tag{14a}$$

$$E_z = -\frac{\partial \beta}{\partial z} = -\frac{\pi}{h_e}\sin\left[\frac{\pi}{h_e}\left(z-\frac{h_m}{2}\right)\right]\beta. \tag{14b}$$

2.3 porous grapheme face sheets

The mathematical modeling and formulation of material properties of FG-porous layers, is considered as two distribution functions as shown in Fig.2.
Material properties of top and bottom facesheets can be written as [39]:

$$E^t(z) = \begin{cases} E_1\left\{1-\xi\cos\left[\dfrac{\pi}{h_g}\left(z-\dfrac{h_m}{2}-h_e-\dfrac{h_g}{2}\right)\right]\right\} & symmetric\ porosity \quad t=top\ sheet \\[4mm] E_1\left\{1-\zeta\cos\left[\dfrac{\pi}{2h_g}\left(z-\dfrac{h_m}{2}-h_e-\dfrac{h_g}{2}\right)+\dfrac{\pi}{4}\right]\right\} & asymmetric\ porosity \end{cases} \tag{15}$$

$$G^t(z) = \begin{cases} G_1\left\{1-\xi\cos\left[\dfrac{\pi}{h_g}\left(z-\dfrac{h_m}{2}-h_e-\dfrac{h_g}{2}\right)\right]\right\} & symmetric\ porosity \quad t=top\ sheet \\[4mm] G_1\left\{1-\zeta\cos\left[\dfrac{\pi}{2h_g}\left(z-\dfrac{h_m}{2}-h_e-\dfrac{h_g}{2}\right)+\dfrac{\pi}{4}\right]\right\} & asymmetric\ porosity \end{cases} \tag{16}$$

$$\rho^t(z) = \begin{cases} \rho_1\left\{1-\xi\cos\left[\dfrac{\pi}{h_g}\left(z-\dfrac{h_m}{2}-h_e-\dfrac{h_g}{2}\right)\right]\right\} & symmetric\ porosity \quad t=top\ sheet \\[2em] \rho_1\left\{1-\zeta\cos\left[\dfrac{\pi}{2h_g}\left(z-\dfrac{h_m}{2}-h_e-\dfrac{h_g}{2}\right)+\dfrac{\pi}{4}\right]\right\} & asymmetric\ porosity \end{cases} \tag{17}$$

$$E^b(z) = \begin{cases} E_1\left\{1-\xi\cos\left[\dfrac{\pi}{h_g}\left(z-\dfrac{h_m}{2}-h_e-\dfrac{h_g}{2}\right)\right]\right\} & symmetric\ porosity \quad b=bottom\ sheet \\[2em] E_1\left\{1-\zeta\cos\left[\dfrac{\pi}{2h_g}\left(z-\dfrac{h_m}{2}-h_e-\dfrac{h_g}{2}\right)+\dfrac{\pi}{4}\right]\right\} & asymmetric\ porosity \end{cases} \tag{18}$$

$$G^b(z) = \begin{cases} G_1\left\{1-\xi\cos\left[\dfrac{\pi}{h_g}\left(z-\dfrac{h_m}{2}-h_e-\dfrac{h_g}{2}\right)\right]\right\} & symmetric\ porosity \quad b=bottom\ sheet \\[2em] G_1\left\{1-\zeta\cos\left[\dfrac{\pi}{2h_g}\left(z-\dfrac{h_m}{2}-h_e-\dfrac{h_g}{2}\right)+\dfrac{\pi}{4}\right]\right\} & asymmetric\ porosity \end{cases} \tag{19}$$

$$\rho^b(z) = \begin{cases} \rho_1\left\{1-\xi\cos\left[\dfrac{\pi}{h_g}\left(z-\dfrac{h_m}{2}-h_e-\dfrac{h_g}{2}\right)\right]\right\} & symmetric\ porosity \quad b=bottom\ sheet \\[2em] \rho_1\left\{1-\zeta\cos\left[\dfrac{\pi}{2h_g}\left(z-\dfrac{h_m}{2}-h_e-\dfrac{h_g}{2}\right)+\dfrac{\pi}{4}\right]\right\} & asymmetric\ porosity \end{cases} \tag{20}$$

where ζ denotes porosity index and ξ describes mass density which can be expressed as [40]:

$$\xi = 1-\sqrt{1-\zeta} \tag{21}$$

Stress in FG-Porous core can be defined as [41]:

$$\begin{bmatrix} \sigma_{xx} \\ \sigma_{xz} \end{bmatrix} = \begin{bmatrix} Q_{11} & 0 \\ 0 & Q_{55} \end{bmatrix}\begin{bmatrix} \varepsilon_x \\ \gamma_{xz} \end{bmatrix}, \tag{22}$$

The parameters Q_{11} and Q_{55} can be given by [42]:

$$Q_{11} = \frac{E}{1-v}, Q_{55} = G_{12}, \tag{23}$$

in which, E and G_{12} represent longitudinal elastic modulus and shear modulus. Also, v is Poisson's ratio.

2.4 Silica Aerogel Foundation

Based on the Silica Aerogel foundation model, the strain energy can be written as [43]:

$$U_{foundation} = \frac{b}{2} \int_{-\infty}^{\infty} \int_{0}^{H} \left(\partial_{xx} f_{xx} + \partial_{zz} f_{zz} + \partial_{xz} f_{xz} \right) dz dx, \tag{24}$$

Where $\partial_{xx}, \partial_{xz}, \partial_{zz}, f_{xx}, f_{zz}$ and f_{xz} are the stresses and the strains corresponding to the foundation. The displacements of foundation is assumed as [43]:

$$u(\text{x},\text{z},\text{t}) = 0, \tag{25}$$

$$W(x,z,t) = w(x,t)\chi(z), \tag{26}$$

in which $w(x,t)$ is transverse displacement in mid-surface of micro beam and $\chi(z)$ is the shape function of foundation with following boundary conditions [44]:

$$\chi(-H) = 0 \qquad \chi(0) = 1, \tag{27}$$

According to the described displacement field in the foundation, strains are derived as [44]:

$$f_{xx} = \frac{\partial U}{\partial x} = 0 \tag{28}$$

$$f_{zz} = \frac{\partial w}{\partial z} = w(x) \frac{\partial \chi(z)}{\partial z} \tag{29}$$

$$f_{xz} = \frac{\partial u}{\partial z} + \frac{\partial w}{\partial x} = \chi(z) \frac{\partial w}{\partial x} \tag{30}$$

By substituting Eqs. (28-30) in Eq. (24):

$$U_{foundation} = \frac{b}{2} \int_{-\infty}^{\infty} \int_{0}^{H} \left[\frac{E_f(1-v_f)}{(1+v_f)(1-2v_f)} w^2(x) \left(\frac{d\chi}{dz}\right)^2 + \frac{E_f}{2(1+v_f)} \chi^2(z) \left(\frac{dw}{dx}\right)^2 \right] dz dx, \tag{31}$$

By minimizing the function $U_{foundation}$, the following relations can be obtained [45]:

$$k_1 w - k_2 \frac{\partial^2 W}{\partial x^2} = 0 \tag{32}$$

$$k_1 = \frac{b}{2} \int_{-\infty}^{\infty} \int_{0}^{H} \frac{E_f \chi^2(z)}{2(1+v_c)} dz dx, \tag{33}$$

$$k_2 = \frac{b}{2} \int_{-\infty}^{\infty} \int_{0}^{H} \frac{E_f(1-v_f)}{(1+v_c)(1-2v_c)} \left(\frac{d\chi}{dz}\right)^2 dz dx, \tag{34}$$

Where k_1 and k_2 are the shear and compression foundation parameters, respectively [45]:

$$\chi(z) = \frac{\sinh\left[\gamma\left(1-\frac{z}{H}\right)\right]}{\sinh(\gamma)}, \tag{35}$$

$$\gamma^2 = h^2 \frac{\left(1-2v_f\right)\int\limits_{-\infty}^{+\infty}\left(\frac{dw}{dx}\right)^2 dx}{2\left(1-v_f\right)\int\limits_{-\infty}^{+\infty} w^2(x)dx} \tag{36}$$

2.5 Hamilton's principle

The governing equations of motion using the Hamilton principle for sandwich micro beam rested on Silica Aerogel foundation exposed to the external forces can be calculated as [46]:

$$\delta \int\limits_{t_1}^{t_2} \left[U-\left(K+\Sigma\right)\right]dt = 0 \tag{37}$$

Where U, K and Σ are strain energy, kinetic energy and work done by external work, respectively. The electrostatic -magneto energy U that occupying region Λ is given by [47]:

$$U_{SMB} = \frac{1}{2}\int\limits_{\Lambda}\left[\sigma_{ij}\varepsilon_{ij}-B_iH_i-D_iE_i+p_i\gamma_i+\tau_{ijk}^{(1)}\eta_{ijk}^{(1)}+m_{ij}\chi_{ij}\right]d\Lambda, \tag{38}$$

In which, γ_i, $\eta_{ijk}^{(1)}$ and χ_{ij} represent the dilatation gradient vector, deviatoric stretch gradient and symmetric rotation gradient tensors, respectively, and p_i, $\tau_{ijk}^{(1)}$ and m_{ij} are the higher-order stresses [48,49].

$$\varepsilon_{ij} = \frac{1}{2}\left(\frac{\partial u_j}{\partial x_i}+\frac{\partial u_i}{\partial x_j}\right), \tag{39}$$

$$\gamma_i = \frac{\partial \varepsilon_{mm}}{\partial x_i}, \tag{40}$$

$$\eta_{ijk}^{(1)} = \frac{1}{3}\left(\frac{\partial \varepsilon_{jk}}{\partial x_i}+\frac{\partial \varepsilon_{ki}}{\partial x_j}+\frac{\partial \varepsilon_{ij}}{\partial x_k}\right)$$
$$-\frac{1}{15}\left[\delta_{ij}\left(\frac{\partial \varepsilon_{mm}}{\partial x_k}+2\frac{\partial \varepsilon_{mk}}{\partial x_m}\right)+\delta_{jk}\left(\frac{\partial \varepsilon_{mm}}{\partial x_i}+2\frac{\partial \varepsilon_{mi}}{\partial x_m}\right)+\delta_{ki}\left(\frac{\partial \varepsilon_{mm}}{\partial x_j}+2\frac{\partial \varepsilon_{mj}}{\partial x_m}\right)\right], \tag{41}$$

$$\chi_{ij} = \frac{1}{2}\left(e_{ipq}\frac{\partial \varepsilon_{qj}}{\partial x_p}+e_{jpq}\frac{\partial \varepsilon_{qi}}{\partial x_p}\right), \tag{42}$$

$$p_i = 2l_0^2 G\gamma_i, \tag{43}$$

$$\tau_{ijk}^{(1)} = 2l_1^2 G \eta_{ijk}^{(1)}, \tag{44}$$

$$m_{ij} = 2l_2^2 G \chi_{ij}, \tag{45}$$

where u_i, δ_{ij} and e_{ipq} are the displacement vector, kronecker delta and alternate tensor, respectively, and l_0, l_1 and l_2 indicate the three material length scale parameters. By expanding Eqs. (39-45) and substituting Eqs. (5) and (6) into this equations, the results can be obtained according to Appendix A.

In order to obtain the total strain energy, equations must be written for each layer as [50]:

$$U_{piezomagnet} = \frac{1}{2} \int_0^L \int_{-\frac{h_m}{2}}^{\frac{h_m}{2}} \left(\sigma_{ij}^m \varepsilon_{ij}^m - B_i H_i + p_i \gamma_i + \tau_{ijk}^{(1)} \eta_{ijk}^{(1)} + m_{ij} \chi_{ij} \right) dz\, dx, \tag{46}$$

$$
\begin{aligned}
U_{piezoelectric} = {} & \frac{1}{2} \int_0^L \int_{\frac{h_m}{2}}^{\frac{h_m}{2}+h_e} \left(\sigma_{ij}^e \varepsilon_{ij}^e - D_i E_i + p_i \gamma_i + \tau_{ijk}^{(1)} \eta_{ijk}^{(1)} + m_{ij} \chi_{ij} \right) dz\, dx \\
& + \frac{1}{2} \int_0^L \int_{-\frac{h_m}{2}-h_e}^{-\frac{h_m}{2}} \left(\sigma_{ij}^e \varepsilon_{ij}^e - D_i E_i + p_i \gamma_i + \tau_{ijk}^{(1)} \eta_{ijk}^{(1)} + m_{ij} \chi_{ij} \right) dz\, dx,
\end{aligned}
\tag{47}
$$

$$
\begin{aligned}
U_{graphene} = {} & \frac{1}{2} \int_0^L \int_{\frac{h_m}{2}+h_e}^{\frac{h_m}{2}+h_e+h_c} \left(\sigma_{ij}^c \varepsilon_{ij}^c + p_i \gamma_i + \tau_{ijk}^{(1)} \eta_{ijk}^{(1)} + m_{ij} \chi_{ij} \right) dz\, dx \\
& + \frac{1}{2} \int_0^L \int_{-\frac{h_m}{2}-h_e-h_c}^{-\frac{h_m}{2}-h_e} \left(\sigma_{ij}^c \varepsilon_{ij}^c + p_i \gamma_i + \tau_{ijk}^{(1)} \eta_{ijk}^{(1)} + m_{ij} \chi_{ij} \right) dz\, dx,
\end{aligned}
\tag{48}
$$

The kinetic energy can be developed as follows [50]

$$K_{SMB} = \frac{1}{2} \int_\Lambda \rho \left[\left(\frac{\partial U}{\partial t} \right)^2 + \left(\frac{\partial W}{\partial t} \right)^2 \right] d\Lambda, \tag{49}$$

The kinetic energy of sandwich micro beam can be obtained as following form:

$$K_{piezomagnet} = \frac{1}{2} \int_0^L \int_{-\frac{h_m}{2}}^{\frac{h_m}{2}} \rho_m \left[\left(\frac{\partial U}{\partial t} \right)^2 + \left(\frac{\partial W}{\partial t} \right)^2 \right] dz\, dx, \tag{50}$$

$$K_{piezoelectric} = \frac{1}{2}\int_0^L \int_{\frac{h_m}{2}}^{\frac{h_m}{2}+h_e} \rho_e\left[\left(\frac{\partial U}{\partial t}\right)^2+\left(\frac{\partial W}{\partial t}\right)^2\right]dz\,dx + \frac{1}{2}\int_0^L \int_{-\frac{h_m}{2}-h_e}^{-\frac{h_m}{2}} \rho_e\left[\left(\frac{\partial U}{\partial t}\right)^2+\left(\frac{\partial W}{\partial t}\right)^2\right]dz\,dx, \quad (51)$$

$$K_{graphene} = \frac{1}{2}\int_0^L \int_{\frac{h_m}{2}+h_e}^{\frac{h_m}{2}+h_e+h_c} \rho_c\left[\left(\frac{\partial U}{\partial t}\right)^2+\left(\frac{\partial W}{\partial t}\right)^2\right]dz\,dx$$
$$+\frac{1}{2}\int_0^L \int_{-\frac{h_m}{2}-h_e-h_c}^{-\frac{h_m}{2}-h_e} \rho_c\left[\left(\frac{\partial U}{\partial t}\right)^2+\left(\frac{\partial W}{\partial t}\right)^2\right]dz\,dx, \quad (52)$$

in which ρ_c, ρ_e, ρ_g are the mass densities of piezomagnetic, piezoelectric and porous graphene layers, respectively.

Inserting the displacement components from Eqs. (39-52) into Eq. (37) and putting the coefficients of $\delta u, \delta w, \delta \varphi, \delta \theta, s\alpha$ and $\delta \beta$ equal to zero, the governing equations of motion of sandwich micro beam rested on Silica Aerogel foundation exposed to the multi physical fields can be developed as:

δu :

$$\frac{4}{5}l_1^2 GI_0\frac{\partial^4}{\partial x^4}u(x,t) + 2I_0 l_0^2 G\frac{\partial^4}{\partial x^4}u(x,t) + \frac{4}{5}l_1^2 GI_1\frac{\partial^4}{\partial x^4}\theta(x,t) + 2l_0^2 I_1 G\frac{\partial^4}{\partial x^4}\theta(x,t)$$

$$+2l_0^2 I_8 G\frac{\partial^4}{\partial x^4}\psi(x,t) - \frac{4}{5}l_1^2 GI_{14}\frac{\partial^2}{\partial x^2}\psi(x,t) + \frac{4}{5}l_1^2 GI_8\frac{\partial^4}{\partial x^4}\psi(x,t) - I_7\frac{\partial^2}{\partial x^2}u(x,t)$$

$$-I_7 I_8\left(\frac{\partial^2}{\partial x^2}\psi(x,t)\right) - I_7 I_1\left(\frac{\partial^2}{\partial x^2}\theta(x,t)\right) + I_4\frac{\partial^2}{\partial t^2}\theta(x,t) + I_5\frac{\partial^2}{\partial t^2}\psi(x,t) + I_3\frac{\partial^2}{\partial t^2}u(x,t)$$

$$+\rho_c I_8\frac{\partial^2}{\partial t^2}\psi(x,t) - \frac{I_{15}\pi e_{31}\frac{\partial}{\partial x}\beta(x,t)}{h_e} + \rho_c I_0\left(\frac{\partial^2}{\partial t^2}u(x,t)\right) + \rho_c I_1\left(\frac{\partial^2}{\partial t^2}\theta(x,t)\right)$$

$$-Q_{11}I_8\left(\frac{\partial^2}{\partial x^2}\psi(x,t)\right) - I_0 Q_{11}(\frac{\partial^2}{\partial x^2}u(x,t)) - Q_{11}I_1(\frac{\partial^2}{\partial x^2}\theta(x,t)) - \frac{8}{5}l_1^2 GI_{14}(\frac{\partial^2}{\partial x^2}\psi(x,t))$$

$$+\frac{8}{5}l_1^2 GI_8(\frac{\partial^4}{\partial x^4}\psi(x,t)) + \frac{8}{5}l_1 \rho_c I_1\left(\frac{\partial^2}{\partial t^2}\theta(x,t)\right) + \rho_c I_0\left(\frac{\partial^2}{\partial t^2}u(x,t)\right) + 2l_0^2 GI_1\frac{\partial^4}{\partial x^4}\theta(x,t)$$

$$+\frac{4}{5}l_1^2 GI_8\frac{\partial^4}{\partial x^4}\psi(x,t) + \frac{4}{5}l_1^2 I_1 G\frac{\partial^4}{\partial x^4}\theta(x,t) - \frac{4}{5}l_1^2 GI_{14}\left(\frac{\partial^2}{\partial x^2}\psi(x,t)\right)^2 + 4l_0^2 I_1 G\frac{\partial^4}{\partial x^4}\theta(x,t)$$

$$+4l_0^2 GI_0\frac{\partial^4}{\partial x^4}u(x,t) + \frac{8}{5}l_1^2 GI_0\frac{\partial^4}{\partial x^4}u(x,t) + 2l_0^2 I_8 G\frac{\partial^4}{\partial x^4}\psi(x,t) + 4l_0^2 GI_8\frac{\partial^4}{\partial x^4}\psi(x,t) = 0, \quad (53)$$

δw :

$$-k_s\,I_9 I_{13}\frac{\partial}{\partial x}\psi(x,t)-k_w\,w(x,t)+k_G\frac{\partial^2}{\partial x^2}w(x,t)-\left(\frac{\partial^2}{\partial x^2}w(x,t)\right)N_{xm}-\left(\frac{\partial^2}{\partial x^2}w(x,t)\right)N_{xe}$$

$$+\frac{1}{8}l_2{}^2 GI_{13}\frac{\partial^3}{\partial x^3}\psi(x,t)+\frac{16}{5}l_1{}^2 I_{13}G(\frac{\partial^3}{\partial x^3}\psi(x,t))+\frac{32}{15}l_1{}^2 GI_0(\frac{\partial^4}{\partial x^4}w(x,t))+\frac{1}{8}l_2{}^2 GI_0\frac{\partial^4}{\partial x^4}w(x,t)$$

$$+\frac{16}{5}l_1{}^2 GI_0(\frac{\partial^3}{\partial x^3}\theta(x,t)))-k_s\,I_9\frac{\partial^2}{\partial x^2}w(x,t)-I_3\frac{\partial^2}{\partial t^2}w(x,t)-Q_{55}k_s\,I_{13}\left(\frac{\partial}{\partial x}\psi(x,t)\right)$$

$$+\rho_c I_0\frac{\partial^2}{\partial t^2}w(x,t)+I_{17}e_{15}\left(\frac{\partial^2}{\partial x^2}\beta(x,t)\right)-\frac{1}{4}l_2{}^2 GI_0(\frac{\partial^3}{\partial x^3}\theta(x,t)+\frac{64}{15}l_1{}^2 GI_0(\frac{\partial^4}{\partial x^4}w(x,t)) \tag{54}$$

$$-Q_{55}I_0 k_s(\frac{\partial^2}{\partial x^2}w(x,t))-\frac{1}{4}l_2{}^2 GI_{13}\frac{\partial^3}{\partial x^3}\psi(x,t)+\frac{32}{5}l_1{}^2 GI_{13}(\frac{\partial^3}{\partial x^3}\psi(x,t))+\frac{16}{5}l_1{}^2 GI_0(\frac{\partial^3}{\partial x^3}\theta(x,t))$$

$$-Q_{55}I_0 k_s\frac{\partial^2}{\partial x^2}w(x,t)-\frac{1}{8}l_2{}^2 GI_0(\frac{\partial^3}{\partial x^3}\theta(x,t)+\frac{16}{5}l_1{}^2 I_{13}G(\frac{\partial^3}{\partial x^3}\psi(x,t))+\frac{32}{15}l_1{}^2 GI_0\left(\frac{\partial^4}{\partial x^4}w(x,t)\right)$$

$$-\frac{1}{8}l_2{}^2 GI_0\left(\frac{\partial^3}{\partial x^3}\theta(x,t)\right)+\rho_c I_0(\frac{\partial^2}{\partial t^2}w(x,t)-k_s\,I_9\left(\frac{\partial}{\partial x}\theta(x,t)\right)-Q_{55}k_s\,I_{13}\left(\frac{\partial}{\partial x}\psi(x,t)\right)$$

$$-Q_{55}I_0 k_s\left(\frac{\partial}{\partial x}\theta(x,t)\right)=0;$$

$\delta\beta$:

$$\frac{I_{15}I_8\pi e_{31}\frac{\partial}{\partial x}\psi(x,t)}{h_e}+\frac{I_{15}I_1\pi e_{31}\frac{\partial}{\partial x}\theta(x,t)}{h_e}-\frac{I_{16}\pi^2 h_{33}\beta(x,t)}{h_e{}^2}+\frac{I_{15}\pi e_{31}\frac{\partial}{\partial x}u(x,t)}{h_e} \tag{55}$$

$$+I_{17}e_{15}\left(\frac{\partial^2}{\partial x^2}w(x,t)\right)+I_{18}h_{11}\left(\frac{\partial^2}{\partial x^2}\beta(x,t)\right)+I_{17}e_{15}I_{13}\frac{\partial}{\partial x}\psi(x,t)+I_{17}e_{15}\left(\frac{\partial}{\partial x}\theta(x,t)\right)=0\,,$$

$\delta\varphi$:

$$-\frac{16}{5}l_1^2 I_{13} G(\frac{\partial^3}{\partial x^3}w(x,t))+\frac{4}{5}l_1^2 GI_8(\frac{\partial^4}{\partial x^4}u(x,t))+\frac{32}{15}l_1^2 GI_{11}\psi(x,t)+\frac{1}{8}l_2^2 GI_{11}\psi(x,t)+2l_0^2 I_8 G\frac{\partial^4}{\partial x^4}u(x,t)$$

$$+\frac{4}{5}l_1^2 GI_{12}\frac{\partial^4}{\partial x^4}\psi(x,t)-\frac{4}{5}l_1^2 GI_1 I_{14}\frac{\partial^2}{\partial x^2}\theta(x,t)+2l_0^2 GI_1 I_8\frac{\partial^4}{\partial x^4}\theta(x,t)+\frac{4}{5}l_1^2 GI_8 I_1\frac{\partial^4}{\partial x^4}\theta(x,t)-I_6\frac{\partial^2}{\partial t^2}\psi(x,t)$$

$$+I_5\frac{\partial^2}{\partial t^2}u(x,t)+k_s I_9 I_{13}(\frac{\partial}{\partial x}w(x,t))-\frac{8}{5}l_1^2 GI_8 I_{14}\frac{\partial^2}{\partial x^2}\psi(x,t)+k_s I_9 I_{13}\theta(x,t)+k_s I_9 I_{10}\psi(x,t)$$

$$+I_5 I_1(\frac{\partial^2}{\partial t^2}\theta(x,t))-I_7 I_8(\frac{\partial^2}{\partial x^2}u(x,t))-I_7 I_{12}(\frac{\partial^2}{\partial x^2}\psi(x,t))+\frac{32}{15}l_1^2 GI_{11}\psi(x,t)-\frac{1}{8}l_2^2 GI_{13}\frac{\partial^3}{\partial x^3}w(x,t)$$

$$-2l_0^2 GI_{13}\frac{\partial^2}{\partial x^2}\theta(x,t)+\frac{4}{5}l_1^2 GI_{12}(\frac{\partial^4}{\partial x^4}\psi(x,t))+2l_0^2 GI_{12}(\frac{\partial^4}{\partial x^4}\psi(x,t))-\frac{16}{5}l_1^2 I_{13} G(\frac{\partial^3}{\partial x^3}w(x,t))$$

$$-\frac{24}{5}l_1^2 GI_{13}(\frac{\partial^2}{\partial x^2}\theta(x,t))-\frac{1}{8}l_2^2 GI_{10}(\frac{\partial^2}{\partial x^2}\psi(x,t))-\frac{24}{5}l_1^2 GI_{10}(\frac{\partial^2}{\partial x^2}\psi(x,t))-\frac{1}{8}l_2^2 GI_{13}\frac{\partial^2}{\partial x^2}\theta(x,t)$$

$$-2l_0^2 GI_{10}\frac{\partial^2}{\partial x^2}\psi(x,t)+2l_0^2 I_8 G\frac{\partial^4}{\partial x^4}u(x,t)-I_7 I_1 I_8(\frac{\partial^2}{\partial x^2}\theta(x,t))-\frac{4}{5}l_1^2 GI_{14}\frac{\partial^2}{\partial x^2}u(x,t)+\frac{1}{8}l_2^2 GI_{11}\psi(x,t)$$

$$-I_{17}e_{15}I_{13}(\frac{\partial}{\partial x}\beta(x,t))+Q_{55}k_s I_{13}\left(\frac{\partial}{\partial x}w(x,t)\right)+Q_{55}k_s I_{13}\theta(x,t)+Q_{55}k_s I_{10}\psi(x,t)+\rho_c I_1 I_8\frac{\partial^2}{\partial t^2}\theta(x,t)$$

$$+\rho_c I_{15}\frac{\partial^2}{\partial t^2}\psi(x,t)-Q_{11}I_8\frac{\partial^2}{\partial x^2}u(x,t)-Q_{11}I_8 I_1\left(\frac{\partial^2}{\partial x^2}\theta(x,t)\right)-Q_{11}I_{12}(\frac{\partial^2}{\partial x^2}\psi(x,t))-\frac{1}{8}l_2^2 GI_{13}\frac{\partial^2}{\partial x^2}\theta(x,t)$$

$$(56)$$

$$+\frac{64}{15}l_1^2 GI_{11}\psi(x,t)+\frac{1}{4}l_2^2 GI_{11}\psi(x,t)-\frac{32}{5}l_1^2 GI_{13}(\frac{\partial^3}{\partial x^3}w(x,t))+4l_0^2 GI_8\frac{\partial^4}{\partial x^4}u(x,t)-\frac{1}{4}l_2^2 GI_{10}\frac{\partial^2}{\partial x^2}\psi(x,t)$$

$$+\frac{8}{5}l_1^2 GI_{12}\frac{\partial^4}{\partial x^4}\psi(x,t)-\frac{48}{5}l_1^2 GI_{10}(\frac{\partial^2}{\partial x^2}\psi(x,t))+4l_0^2 GI_{12}\frac{\partial^4}{\partial x^4}\psi(x,t)+\frac{4}{5}l_1^2 GI_8(\frac{\partial^4}{\partial x^4}u(x,t))$$

$$+\frac{4}{5}l_1^2 GI_8 I_1(\frac{\partial^4}{\partial x^4}\theta(x,t))+\rho_c I_{15}\frac{\partial^2}{\partial t^2}\psi(x,t)+\rho_c I_1 I_8\frac{\partial^2}{\partial t^2}\theta(x,t)-4l_0^2 GI_{10}\frac{\partial^2}{\partial x^2}\psi(x,t)-\frac{1}{4}l_2^2 GI_{13}\frac{\partial^2}{\partial x^2}\theta(x,t)$$

$$-2l_0^2 GI_{13}\frac{\partial^2}{\partial x^2}\theta(x,t)+2l_0^2 GI_{12}\frac{\partial^4}{\partial x^4}\psi(x,t)-\frac{1}{8}l_2^2 GI_{10}\frac{\partial^2}{\partial x^2}\psi(x,t)-\frac{24}{5}l_1^2 GI_{10}(\frac{\partial^2}{\partial x^2}\psi(x,t))$$

$$-\frac{16}{5}l_1^2 GI_{14}\frac{\partial^2}{\partial x^2}u(x,t)=0,$$

$s_\theta:$

$$-\frac{1}{8}l_2{}^2 GI_{13}(\frac{\partial^2}{\partial x^2}\psi(x,t)) + \rho_c I_2(\frac{\partial^2}{\partial t^2}\theta(x,t)) - I_{17}f_{15}\left(\frac{\partial}{\partial x}\alpha(x,t)\right) + 4l_0{}^2 I_1 G(\frac{\partial^4}{\partial x^4}u(x,t)))$$

$$+\rho_c I_1(\frac{\partial^2}{\partial t^2}u(x,t)) - l_2{}^2 I_0 G(\frac{\partial^2}{\partial x^2}\theta(x,t)) - 2l_0{}^2 I_0 G(\frac{\partial^2}{\partial x^2}\theta(x,t)) - l_1{}^2 GI_{13}(\frac{\partial^2}{\partial x^2}\psi(x,t))$$

$$+l_0{}^2 GI_2\left(\frac{\partial^4}{\partial x^4}\theta(x,t)\right) k_s I_9 I_{13}\psi(x,t) - I_3 I_2\frac{\partial^2}{\partial t^2}\theta(x,t) + I_5 I_1\frac{\partial^2}{\partial t^2}\psi(x,t) - I_7 I_2\frac{\partial^2}{\partial x^2}\theta(x,t)$$

$$+k_s I_9\theta(x,t) + \frac{4}{5}l_1{}^2 GI_1(\frac{\partial^4}{\partial x^4}u(x,t)) - \frac{1}{8}l_2{}^2 GI_0(\frac{\partial^2}{\partial x^2}\theta(x,t)) + 2l_0{}^2 GI_2(\frac{\partial^4}{\partial x^4}\theta(x,t))$$

$$-2l_0{}^2 GI_{13}(\frac{\partial^2}{\partial x^2}\psi(x,t)) - I_7 I_1\left(\frac{\partial^2}{\partial x^2}u(x,t)\right) + k_s I_9\left(\frac{\partial}{\partial x}w(x,t)\right) + 2l_0{}^2 I_1 G(\frac{\partial^4}{\partial x^4}u(x,t))$$

$$-\frac{1}{8}l_2{}^2 GI_{13}\left(\frac{\partial^2}{\partial x^2}\psi(x,t)\right) - \frac{4}{5}l_1{}^2 GI_1 I_{14}(\frac{\partial^2}{\partial x^2}\psi(x,t)) + \frac{4}{5}l_1{}^2 GI_8 I_1(\frac{\partial^4}{\partial x^4}\psi(x,t)) - \frac{I_{15} I_1\pi e_{31}}{h_e}(\frac{\partial}{\partial x}\beta(x,t))$$

$$+\frac{8}{5}l_1{}^2 GI_8 I_1(\frac{\partial^4}{\partial x^4}\psi(x,t)) + 4l_0{}^2 GI_8 I_1(\frac{\partial^4}{\partial x^4}\psi(x,t)) + Q_{55}k_s I_0\left(\frac{\partial}{\partial x}w(x,t)\right) + Q_{55}I_0 k_s\theta(x,t)$$

$$+Q_{55}k_s I_{13}\psi(x,t) - \frac{8}{5}l_1{}^2 GI_{14} I_1(\frac{\partial^2}{\partial x^2}\psi(x,t))(x,t) - \frac{24}{5}l_1{}^2 GI_0(\frac{\partial^2}{\partial x^2}\theta(x,t)) - \frac{24}{5}l_1{}^2 GI_{13}(\frac{\partial^2}{\partial x^2}\psi(x,t))$$

$$-I_7 I_1 I_8\left(\frac{\partial^2}{\partial x^2}\psi(x,t)\right) - 2l_0{}^2 GI_0(\frac{\partial^2}{\partial x^2}\theta(x,t)) + I_4(\frac{\partial^2}{\partial t^2}u(x,t)) + \frac{1}{8}l_2{}^2 GI_0(\frac{\partial^3}{\partial x^3}w(x,t))$$ (57)

$$-\frac{16}{5}l_1{}^2 GI_0(\frac{\partial^3}{\partial x^3}w(x,t)) - 4l_0{}^2 I_{13} G\left(\frac{\partial^2}{\partial x^2}\psi(x,t)\right) + \frac{4}{5}l_1{}^2 GI_2(\frac{\partial^4}{\partial x^4}\theta(x,t)) + 2l_0{}^2 GI_1 I_8(\frac{\partial^4}{\partial x^4}\psi(x,t))$$

$$-Q_{11}I_8 I_1\frac{\partial^2}{\partial x^2}\psi(x,t) + 2l_0{}^2 GI_1\left(\frac{\partial^4}{\partial x^4}u(x,t)\right) - I_{17}e_{15}\frac{\partial}{\partial x}\beta(x,t) - Q_{11}I_8 I_1\frac{\partial^2}{\partial x^2}\psi(x,t)$$

$$-\frac{1}{4}l_2{}^2 GI_0(\frac{\partial^2}{\partial x^2}\theta(x,t)) - \frac{1}{4}l_2{}^2 GI_{13}\frac{\partial^2}{\partial x^2}\psi(x,t) - 4l_0{}^2 GI_0\left(\frac{\partial^2}{\partial x^2}\theta(x,t)\right) + Q_{55}I_0 k_s\left(\frac{\partial}{\partial x}w(x,t)\right)$$

$$-Q_{11}I_1(\frac{\partial^2}{\partial x^2}u(x,t)) - Q_{11}I_2(\frac{\partial^2}{\partial x^2}\theta(x,t)) + Q_{55}I_0 k_s\theta(x,t) + Q_{55}k_s I_{13}\psi(x,t) + \rho_c I_1 I_8(\frac{\partial^2}{\partial t^2}\psi(x,t))$$

$$+\frac{4}{5}l_1{}^2 GI_2(\frac{\partial^4}{\partial x^4}\theta(x,t)) - \frac{24}{5}l_1{}^2 I_0 G(\frac{\partial^2}{\partial x^2}\theta(x,t)) + l_0{}^2 GI_1 I_8(\frac{\partial^4}{\partial x^4}\psi(x,t)) - \frac{4}{5}l_1{}^2 GI_1 I_{14}(\frac{\partial^2}{\partial x^2}\psi(x,t))$$

$$+\frac{4}{5}l_1{}^2 GI_8 I_1(\frac{\partial^4}{\partial x^4}\psi(x,t)) + \frac{1}{8}l_2{}^2 GI_0\left(\frac{\partial^3}{\partial x^3}w(x,t)\right) + l_1{}^2 GI_{13}(\frac{\partial^2}{\partial x^2}\psi(x,t)) - 2l_0{}^2 GI_{13}(\frac{\partial^2}{\partial x^2}\psi(x,t)) = 0,$$

s_α :

$$I_{17}f_{15}\left(\frac{\partial}{\partial x}\theta(x,t)\right)+\frac{I_{15}\pi f_{31}}{h_m}(\frac{\partial}{\partial x}u(x,t))+I_{17}f_{15}\left(\frac{\partial^2}{\partial x^2}w(x,t)\right)+f_{15}I_{17}I_{13}(\frac{\partial}{\partial x}\psi(x,t))$$

$$-\frac{I_{16}\pi^2\mu_{33}\alpha(x,t)}{h_m^2}+\frac{I_8 I_{15}\pi f_{31}}{h_m}(\frac{\partial}{\partial x}\psi(x,t))+\frac{I_{15}I_1\pi f_{31}}{h_m}(\frac{\partial}{\partial x}\theta(x,t))+I_{18}\mu_{11}\frac{\partial^2}{\partial x^2}\alpha(x,t)=0,$$

(58)

where I_i is defined in Appendix B. Also, N_x^m and N_x^e are the normal forces induced by magnetic potential and external electric voltage, respectively, which can be stated as [50]:

$$N_x^m = -2\,f_{31}\,\Omega,$$

(59)

$$N_x^e = -2\,e_{31}\,V_0.$$

Also, the dimensionless parameters are defined to obtain dimensionless results as follows:

$$(\overline{u},\overline{w},\theta,\varphi)=\left(\frac{u}{L},\frac{w}{h_c},\theta,\varphi\right),(\overline{x},\overline{z})=\left(\frac{x}{L},\frac{z}{h_c}\right),\overline{t}=\frac{t}{L}\sqrt{\frac{E_m}{\rho_m}},\overline{C}_{ij}=\frac{c_{ij}}{c_m},\overline{\rho}_{ij}=\frac{\rho_{ij}}{\rho_m},\overline{G}_{ij}=\frac{G_{ij}}{G_m},$$

$$\overline{H}=\frac{H.f_{31}}{E_m.h_m},\overline{E}=\frac{E.e_{31}}{E_m.h_m},\Gamma=\frac{L}{h_c},\gamma=\frac{h_i}{h_c},\overline{K}_{\mathrm{w}}=\frac{k_{\mathrm{w}}.h_c}{E_m},i^*=\frac{i}{h_c},\mathrm{w}^*=\frac{w}{h_c},\overline{K}_{\mathrm{G}}=\frac{k_{\mathrm{G}}.h_c}{E_m},\overline{f}_{ij}=\frac{f_{ij}}{f_{31}},$$

(60)

$$\overline{e}_{ij}=\frac{e_{ij}}{e_{31}},l^*=\frac{l}{h},\omega^*=\frac{\omega L^2}{h}\sqrt{\frac{\rho}{E}},\overline{\mu}_{ij}=\frac{\mu_{ij}.E_m}{f_{31}^2},\overline{h}_{ij}=\frac{h_{ij}.E_m}{e_{31}^2},\overline{N}_{\mathrm{e}}=\frac{N_e}{E_c h_c},\overline{N}_{\mathrm{m}}=\frac{N_m}{E_c h_c},\overline{N}_T=\frac{N_T}{E_c h_c}.$$

3 SOLUTION

According to the Navier's solution, the displacements are considered as functions which satisfy simply support boundary conditions. Therefore, the displacement variables can be expressed as [51]:

$$U(\mathrm{x},\mathrm{t})=\sum_{m=1}^{\infty}U_m(t)\cos(\lambda x),$$

(61)

$$\mathrm{W}(\mathrm{x},\mathrm{t})=\sum_{m=1}^{\infty}w_m(t)\sin(\lambda x),$$

(62)

$$\psi(\mathrm{x},\mathrm{t})=\sum_{m=1}^{\infty}\psi_m(t)\cos(\lambda x),$$

(63)

$$\theta(\mathrm{x},\mathrm{t})=\sum_{m=1}^{\infty}\theta_m(t)\cos(\lambda x),$$

(64)

$$\alpha(x,t) = \sum_{m=1}^{\infty} \alpha_m(t)\sin(\lambda x), \tag{65}$$

$$\beta(x,t) = \sum_{m=1}^{\infty} \beta_m(t)\sin(\lambda x), \tag{66}$$

$$N_T(x,t) = \sum_{m=1}^{\infty} N_T(t)\sin(\lambda x), \tag{67}$$

where $\lambda = \dfrac{m\pi}{L}$ and m is the half wave numbers in the x directions. Inserting the Eqs. (61-67) into Eqs. (53-58), the following equations can be obtained in a matrix form as:

$$\left[M_m\right]\left[\ddot{\Delta}_m\right]+\left[C_m\right]\left[\dot{\Delta}_m\right]+\left[K_m\right]\left[\Delta_m\right]=\left[F_m\right] \tag{68}$$

where, F_{mn} for distribution of thermal loads can be presented as:

$$F_m = \frac{4N^T}{m\pi^2} \tag{69}$$

Where

$$N_c^T = \int E_c \alpha \Delta T dz \tag{70}$$

$$N_e^T = \int E_e \alpha \Delta T dz \tag{71}$$

$$N_g^T = \int E_g \alpha \Delta T dz \tag{72}$$

$$N^T = 2N_g^T + 2N_e^T + N_m^T \tag{73}$$

where $\left[\Delta_m\right]=\left[U_m,W_m,\theta_m,\psi_m,\alpha_m,\beta_m\right]$ is the displacement vector. The [M], [C] and [K] are the mass, damping and stiffness matrices, respectively. For the dynamic bending analysis, Eq. (68) must be solved by using the Laplace transformation. Performing the Laplace transform on Eq. (68) and considering zero initial conditions at the initial time (namely, $\left[\Delta_m\right]=\left[\dot{\Delta}_m\right]=0$ at $t=0$), yields a new system of equations in which time dependency is eliminated as follows:

$$\left[L_{mn}\right]\left[\overline{\Delta}\right]=\left[F_{mn}\right], \quad L_{mn} = K_{mn} + s\,C_{mn} + s^2 M_{mn}. \tag{74}$$

Here, S is the Laplace transform parameter and the bar superscript indicates transformed quantities. The elements of matrix [L_{ij}] are given in Appendix C. By solving Eq. (74), each component of the displacement vector can be derived in the Laplace domain.

4 VERIFICATION

To verify the present formulation, a comparison is carried out for dynamic thermal response of simply supported sandwich micro beam. Geometric properties of beam are considered as h_c=1μm and the material properties are $E^c = 200 Gpas$, $\upsilon = 0.33$, $\rho^C = 7850 Kg/m3$, $\rho_p = 1006 Kg/m3$, $E_p = 1.1 Gpas$ and $\gamma = 1$. Table 1 shows the dimensionless deflection which are compared with results of Hajmohammad et al [52].

5 NUMERICAL RESULTS AND DISCUSSION

In this section, detailed case studies are carried out to investigate the influences of length-to-thickness ratio, layer thickness ratio, piezomagnetic and piezoelectric fields on dynamic thermal stability. According to Tables 2 and 4, BaTiO3 and CoFe2O4 are chosen for piezo-electric layers and piezo-magnetic core, respectively.

In order to obtain results, the other parameters are considered as follows:
$h_t = h_c = h_b = 1\mu m, L = 10\mu m, l_0 = l_1 = l_2 = 10^{-6}, b = 0.2\mu m, \zeta = 0.4, T = 100$.

Fig.3. shows the effect of the various length-to-thickness ratios on dynamic response of sandwich micro beam (SMB) under thermal load. It is obvious that increasing the length of SMB when thickness is constant causes to an increase in dynamic deflection. By increasing the values of l^*, mass of the micro beam increases and its stiffness decreases; thus, dynamic eflection of the micro beam grows. Fig. 3 shows that 30% increase in l^* leads to 60% decrase in the maximum deflection of the nano beam.

Fig.4. shows the effect of the elastic foundation on dynamic response of SMB under thermal load. It can be seen, considering Silica Aerogel foundation decreases dynamic deflection of SMB. It is due to the fact that considering elastic foundation leads to a stiffer micro beam. Consequently, existence of elastic foundation reduces the dynamic deflection of the micro beam.
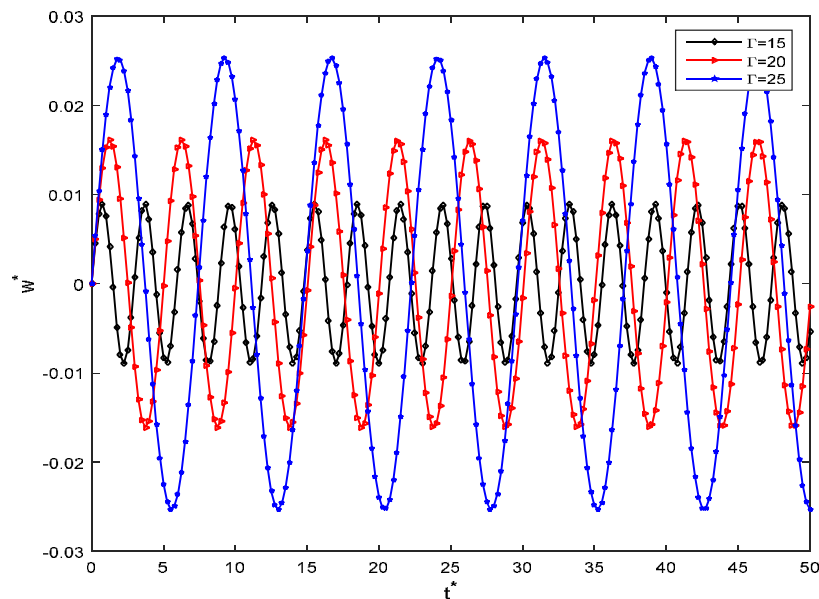
Fig. 3
Effect of various length-to-thickness ratio on dynamic response of SMB under thermal load.
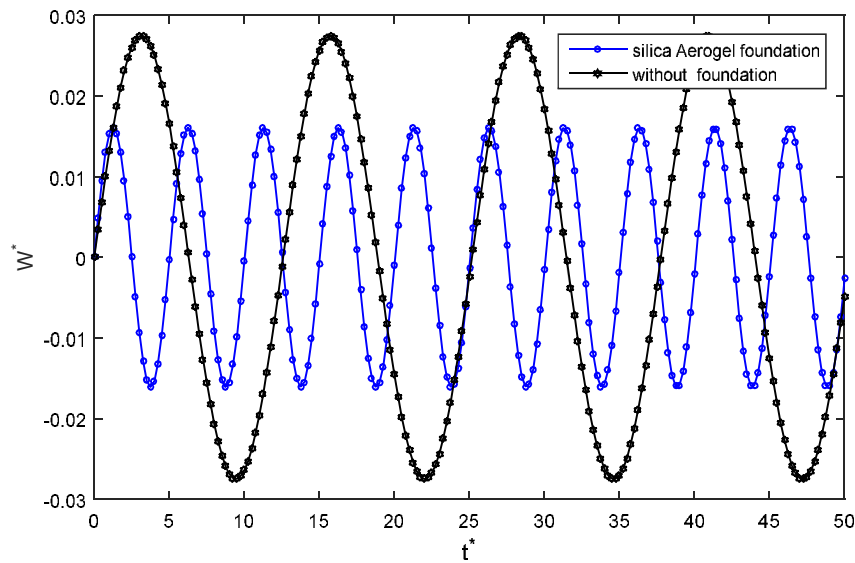
Fig. 4
Effect of Silica Aerogel foundation on dynamic response of SMB under thermal load.

Fig.5. shows the effect of the various thermal loads on dynamic response of SMB. Increase in temperature generates a higher compressive axial load which reduces the stiffness of the micro beam and increases in dynamic deflection. Fig. 5 shows that 100% increase in the temperature elevation leads to 90% increase in the maximum deflection of the micro beam.

Fig.6. shows the effect of the MCST and MSGT on dynamic response of SMB under thermal load. If three material length scale parameters become equal to zero, CT is achieved, therefore, there is a discrepancy between the results of different theories including MSGT ($l_0, l_1, l_2 \neq 0$), MCST ($l_0 = l_1 = 0 \ and \ l_2 \neq 0$). As shown in Fig. 6, the dynamic response of SMB obtained by MCST is lower than that of MSGT. This means that the SMB becomes stiffer or the size effect at micro scale causes to this increase. In comparison with MCST, increase in the material length scale parameters leads to higher molecular interaction force which creates higher stiffness and reduces the dynamic deflection.
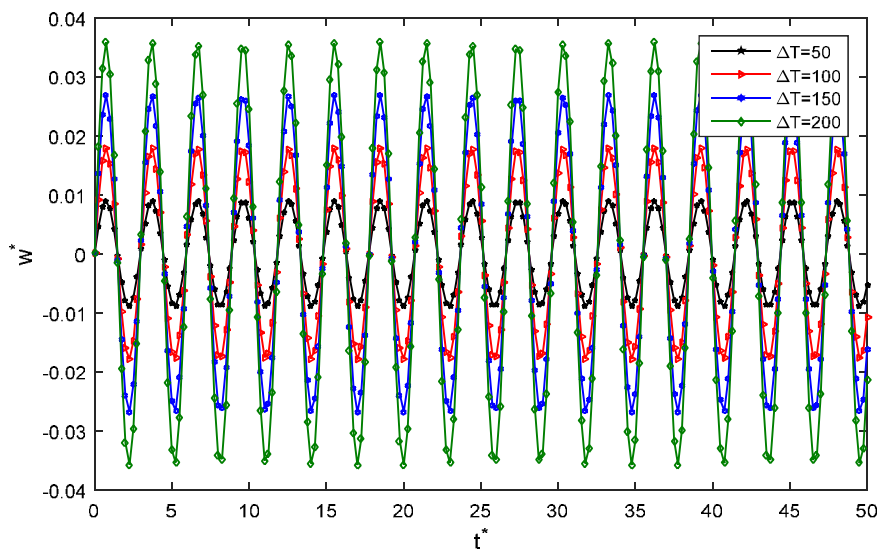
Fig. 5
Effect of temperature changes on dynamic response of SMB.
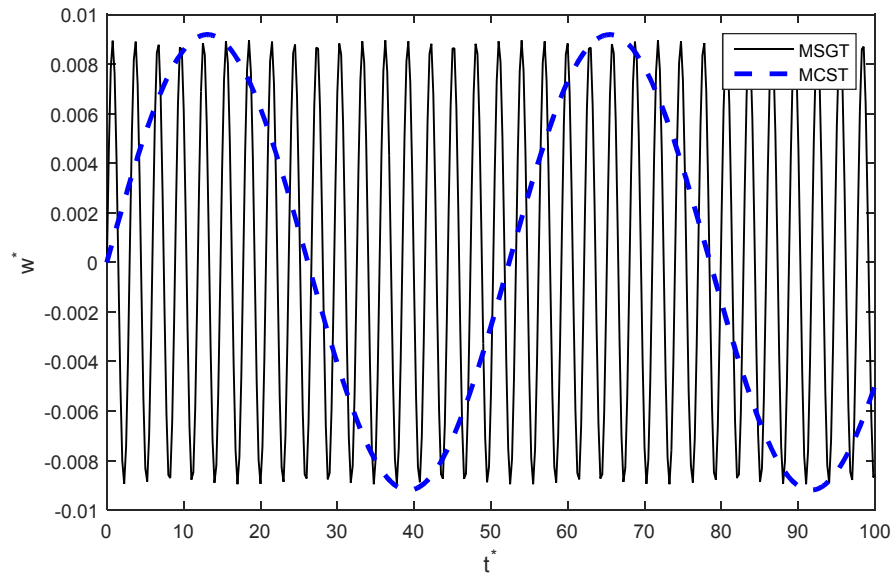
Fig. 6
Effect of MCST and MSGT on dynamic response of SMB.

Fig.7. shows the effect of different mode numbers on dynamic response of SMB under thermal load. Also, dynamic deflection of first mode is more than other modes. By increasing the mode number, the natural frequency of the micro beam increases due to the growth in the stiffness; thus, increase in the mode number reduces the dynamic deflection of the micro beam.

Fig.8. shows the effect of various FG porosity on dynamic response of SMB. It is obvious that dynamic deflection of SMB in asymmetric porosity is lower than that of symmetric porosity. In the symmetric porosity the micro beam benefits from higher stiffness due to the symmetric distribution of the pores; thus, the dynamic deflection for the symmetric porosity is less then the dynamic deflection for the asymmetric porosity.
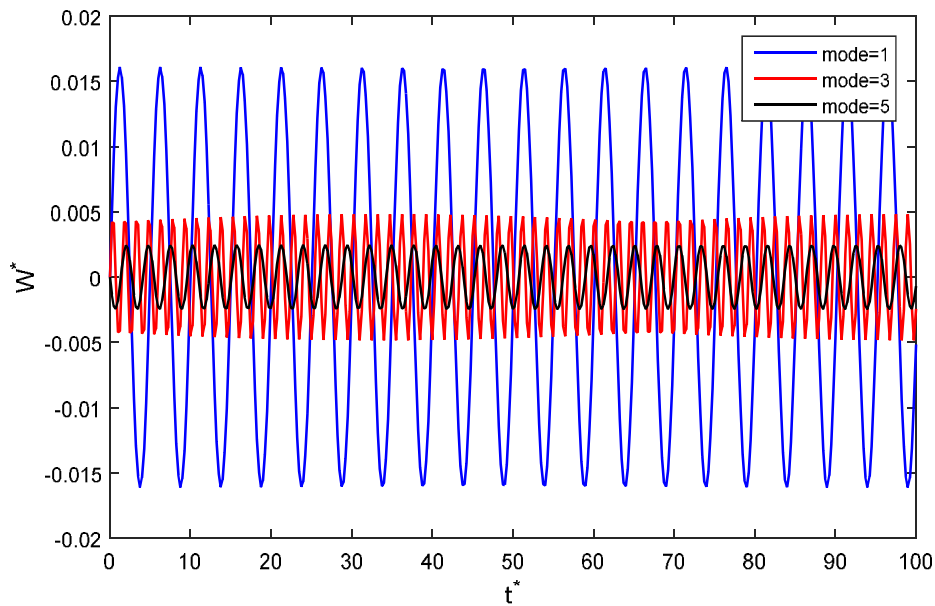
Fig. 7
Effect of different mode numbers on dynamic response of SMB under thermal load.
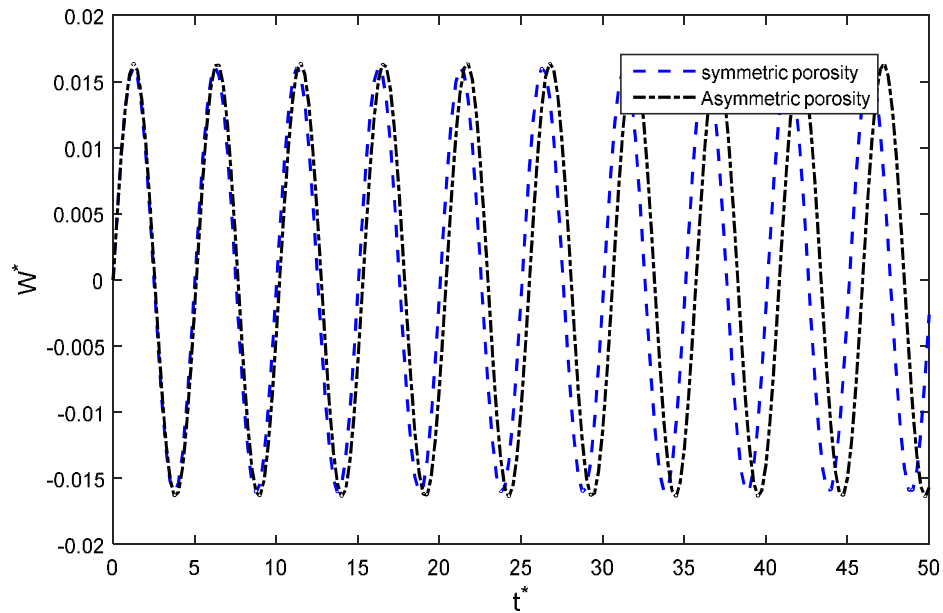
Fig. 8
Effect of various FG porosity on dynamic response of SMB under thermal load.
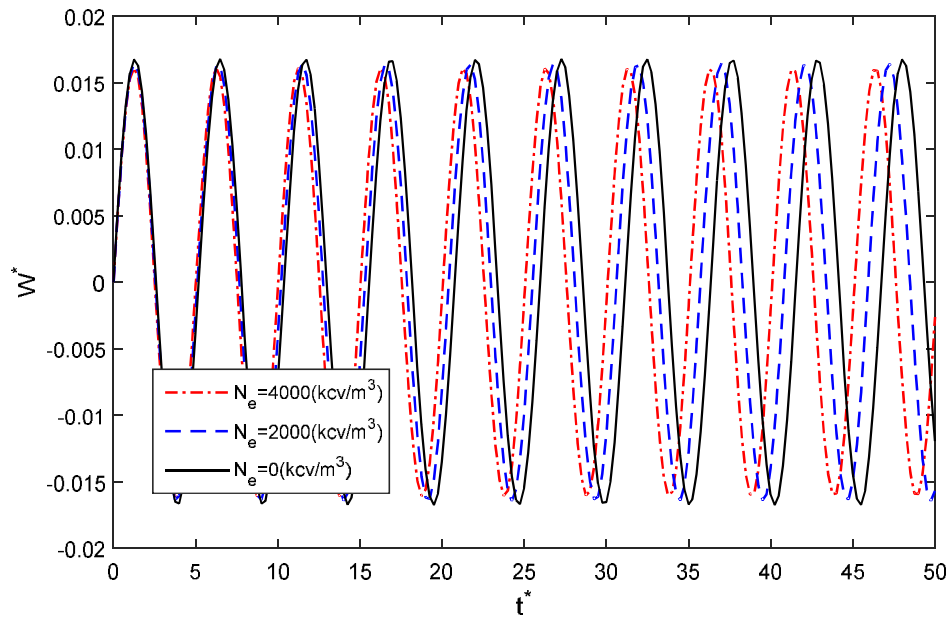
Fig. 9
Effect of various electric loading on dynamic response of SMB under thermal load.

Fig.9. shows the effect of various electric loading on dynamic response of SMB under thermal load. As it can be seen in this figure, by increasing the voltage which is applied on face-sheets, the dynamic response increases. That is due to the fact that the biaxial compressive and tensile forces will be generated in the sandwich micro-beam by applying positive.
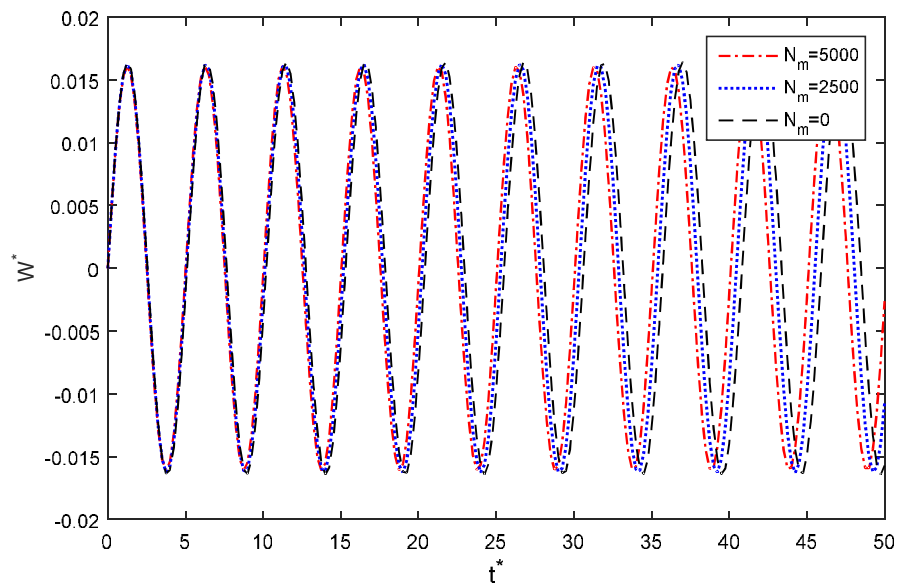
Fig. 10
Effect of various magnetic loadings on dynamic response of SMB under thermal load.

Fig.10. shows the effect of various magnetic loadings on dynamic response of SMB under thermal load. As it can be seen from this figure, by increasing the magnetic loadings which is applied on face-sheets, the dynamic response increases. Piezo-electric and piezo-magnet forces reduces the stiffness of the micro beam; thus by increasing he applied voltage or magnetic field intensity the dynamic deflection of the micro beam increases.

6   CONCLUSIONS

This paper presented transient analysis of simply-supported sandwich micro beam (SMB) with piezo-magnetic core and piezo-electric and porous graphene facesheets resting on Silica Aerogel foundation subjected to the thermal loads. The zigzag deformation beam theory is adopted to model displacement field of SMB. In order to consider size effect, modified strain gradient theory are utilized. The size-dependent equations of motion are derived through Hamilton's principle and solved by iterative technique. From the obtained results, the following conclusions can be drawn:

1) Existence of Silica Aerogel foundation is an important factor for decreasing the dynamic deflection of the micro beam.
2) The dynamic deflection of SMB obtained by MCST is lower than that of MSGT. This means that SMB becomes stiffer or the size effect at micro scale causes to this increase.
3) By increasing the voltage which applied on face-sheets, the dynamic deflection increase.
4) By increasing the magnetic loadings which applied on core, the dynamic deflection increase.
5) Dynamic deflection of SMB in asymmetric porosity is lower than that of symmetric porosity.

APPENDIX A

$$\eta_{xxx} = \frac{\partial e_{xx}}{\partial x} - \frac{1}{5}\left(\frac{\partial e_{xx}}{\partial x} + 2\frac{\partial e_{xx}}{\partial x} + \frac{\partial e_{xz}}{\partial z}\right) = 2/5\frac{\partial^2}{\partial x^2}u(x,t) + 2/5z\frac{\partial^2}{\partial x^2}\theta(x,t)$$
$$+2/5Q_1(z)\frac{\partial^2}{\partial x^2}\psi(x,t) - 2/5\left(\frac{d^2}{dz^2}Q_1(z)\right)\psi(x,t) \tag{A-1}$$

$$\eta_{xxz} = \frac{1}{3}\left(2\frac{\partial e_{xz}}{\partial x} + \frac{\partial e_{xx}}{\partial z}\right) - \frac{1}{15}\left(\frac{\partial e_{xx}}{\partial z} + 2\frac{\partial e_{xz}}{\partial z}\right) = \frac{8\frac{\partial^2}{\partial x^2}w(x,t)}{15} + 4/5\frac{\partial}{\partial x}\theta(x,t)$$
$$+4/5\left(\frac{d}{dz}Q_1(z)\right)\frac{\partial}{\partial x}\psi(x,t) \tag{A-2}$$

$$\eta_{xyy} = -\frac{1}{15}\left(\frac{\partial e_{xx}}{\partial x} + 2\left(\frac{\partial e_{xx}}{\partial x} + \frac{\partial e_{xz}}{\partial z}\right)\right) = -1/5\frac{\partial^2}{\partial x^2}u(x,t) - 1/5z\frac{\partial^2}{\partial x^2}\theta(x,t)$$
$$-1/5Q_1(z)\frac{\partial^2}{\partial x^2}\psi(x,t) - 2/15\left(\frac{d^2}{dz^2}Q_1(z)\right)\psi(x,t) \tag{A-3}$$

$$\eta_{zzz} = -\frac{1}{5}\left(\frac{\partial e_{xx}}{\partial z} + 2\frac{\partial e_{xz}}{\partial x}\right) = -2/15\frac{\partial^2}{\partial x^2}w(x,t) - 1/5\frac{\partial}{\partial x}\theta(x,t)$$
$$-1/5\left(\frac{d}{dz}Q_1(z)\right)\frac{\partial}{\partial x}\psi(x,t) \tag{A-4}$$

$$\eta_{xzz} = \frac{1}{3}\left(2\frac{\partial e_{xz}}{\partial z}\right) - \frac{1}{15}\left(\frac{\partial e_{xx}}{\partial x} + 2\left(\frac{\partial e_{xx}}{\partial x} + \frac{\partial e_{xz}}{\partial z}\right)\right) = \frac{8\left(\frac{d^2}{dz^2}Q_1(z)\right)\psi(x,t)}{15}$$
$$-1/5\frac{\partial^2}{\partial x^2}u(x,t) - 1/5z\frac{\partial^2}{\partial x^2}\theta(x,t) - 1/5Q_1(z)\frac{\partial^2}{\partial x^2}\psi(x,t) \tag{A-5}$$

$$\eta_{yyz} = -\frac{1}{15}\left(\frac{\partial e_{xx}}{\partial z} + 2\frac{\partial e_{xz}}{\partial x}\right) = -2/5\frac{\partial^2}{\partial x^2}w(x,t) - 3/5\frac{\partial}{\partial x}\theta(x,t)$$
$$-3/5\left(\frac{d}{dz}Q_1(z)\right)\frac{\partial}{\partial x}\psi(x,t) \tag{A-6}$$

$$\tau_{xxx} = \left(2l_1^2 G\right)\eta_{xxx} \tag{A-7}$$

$$\tau_{xyy} = \left(2l_1^2 G\right)\eta_{xyy} \tag{A-8}$$

$$\tau_{xxz} = \left(2l_1^2 G\right)\eta_{xxz} \tag{A-9}$$

$$\tau_{xzz} = \left(2l_1^2 G\right)\eta_{zzx} \tag{A-10}$$

$$\tau_{yyz} = \left(2l_1^2 G\right)\eta_{yyz} \tag{A-11}$$

$$\tau_{zzz} = \left(2l_1^2 G\right)\eta_{zzz} \tag{A-12}$$

$$p_x = \left(2l_0^2 G\right)\gamma_x \tag{A-13}$$

$$p_z = \left(2l_0^2 G\right)\gamma_z \tag{A-14}$$

$$\chi_{xy} = \frac{1}{2}\left(-\frac{1}{2}\frac{\partial \gamma_{xz}}{\partial x} + \frac{\partial e_{xx}}{\partial z}\right) = -1/4\frac{\partial^2}{\partial x^2}w(x,t) + 1/4\frac{\partial}{\partial x}\theta(x,t)$$
$$+1/4\left(\frac{\mathrm{d}}{\mathrm{d}z}Q_1(z)\right)\frac{\partial}{\partial x}\psi(x,t) \tag{A-15}$$

$$\chi_{yz} = \frac{1}{2}\left(\frac{1}{2}\frac{\partial \gamma_{xz}}{\partial z}\right) = 1/4\left(\frac{\mathrm{d}^2}{\mathrm{d}z^2}Q_1(z)\right)\psi(x,t) \tag{A-16}$$

$$m_{xy} = \left(2l_2^2 G\right)\chi_{xy} \tag{A-17}$$

$$m_{xy} = \left(2l_2^2 G\right)\chi_{xy} \tag{A-18}$$

$$m_{yz} = \left(2l_2^2 G\right)\chi_{yz} \tag{A-19}$$

$$\gamma_x = \frac{\partial}{\partial x}e_{xx} = \frac{\partial^2}{\partial x^2}u(x,t) + z\frac{\partial^2}{\partial x^2}\theta(x,t) + Q_1(z)\frac{\partial^2}{\partial x^2}\psi(x,t) \tag{A-20}$$

$$\gamma_z = \frac{\partial}{\partial z}e_{zz} = \frac{\partial}{\partial x}\theta(x,t) + \left(\frac{\mathrm{d}}{\mathrm{d}z}Q_1(z)\right)\frac{\partial}{\partial x}\psi(x,t) \tag{A-21}$$

APPENDIX B

$$I_0 = \int dz \tag{B-1}$$

$$I_1 = \int z\,dz \tag{B-2}$$

$$I_2 = \int z^2\,dz \tag{B-3}$$

$$I_3 = \int \rho_C(z)\,dz \tag{B-4}$$

$$I_4 = \int z.\rho_C(z)\,dz \tag{B-5}$$

$$I_5 = \int Q_1(z).\rho_C(z)dz \tag{B-6}$$

$$I_6 = \int Q_1(z)^2.\rho_C(z)dz \tag{B-7}$$

$$I_7 = \int C_{11}(z)dz \tag{B-8}$$

$$I_8 = \int Q_1(z)dz \tag{B-9}$$

$$I_9 = \int_{-\frac{h}{2}}^{\frac{h}{2}} C_{55}(z)dz \tag{B-10}$$

$$I_{10} = \int (\frac{d\,Q_1(z)}{dz})^2 dz \tag{B-11}$$

$$I_{11} = \int_{-\frac{h}{2}}^{\frac{h}{2}} (\frac{d^2 Q_1(z)}{dz^2})^2 dz \tag{B-12}$$

$$I_{12} = \int Q_1(z)^2 dz \tag{B-13}$$

$$I_{13} = \int \frac{d\,Q_1(z)}{dz} dz \tag{B-14}$$

$$I_{14} = \int \frac{d^2 Q_1(z)}{dz^2} dz \tag{B-15}$$

$$I_{15} = \int \sin(\frac{\pi}{h_i}(\bar{z}))dz \qquad i = e, \mathrm{m} \tag{B-16}$$

$$I_{16} = \int \sin(\frac{\pi}{h_i}(\bar{z}))^2 dz \qquad i = e, \mathrm{m} \tag{B-17}$$

$$I_{17} = \int \cos(\frac{\pi}{h_i}(\bar{z}))\,dz \qquad i = e, m \tag{B-18}$$

$$I_{18} = \int \cos(\frac{\pi}{h_i}(\bar{z}))^2 dz \qquad i = e, m \tag{B-19}$$

APPENDIX C

$$L_{11} = (\frac{I_{3g}}{\rho_c L})S^2 + (\frac{I_{19g}}{E_c L})\lambda^2 - (\frac{C_{11}I_{4e}}{E_c L})\lambda^2 + (\frac{\rho_e I_{0e}}{\rho_c L})S^2 + (\frac{I_{4m}}{L})\lambda^2 + (\frac{I_{0m}}{L})S^2 + (\frac{2C_{55j}i_0^2 I_{0j}}{E_c L^3})\lambda^4 + (\frac{4C_{55j}i_1^2 I_{0j}}{5E_c L^3})\lambda^4 \tag{C-1}$$

$$L_{12} = (\frac{I_{5g}}{\rho_c L^2})S^2 + (\frac{I_{5g}}{E_c L^2})\lambda^2 + (\frac{C_{11e}I_{9e}}{E_c L^2})\lambda^2 + (\frac{\rho_e I_{9e}}{\rho_c L^2})S^2 + (\frac{I_{9m}}{L^2})\lambda^2 + (\frac{I_{9m}}{L^2})S^2 + (\frac{2C_{55j}i_0^2 I_{9j}}{E_c L^4})\lambda^4 + (\frac{4C_{55j}i_1^2 I_{9j}}{5E_c L^4})\lambda^4 \tag{C-2}$$

$$L_{13} = (\frac{I_{4g}}{\rho_c L^2})S^2 + (\frac{I_{14g}}{E_c L^2})\lambda^2 + (\frac{C_{11}I_{1e}}{E_c L^2})\lambda^2 + (\frac{\rho_e I_{1e}}{\rho_c L^2})S^2 + (\frac{I_{1m}}{L^2})\lambda^2 + (\frac{I_{1m}}{L^2})S^2 + (\frac{2C_{55j}i_0^2 I_{1j}}{E_c L^4})\lambda^4 + (\frac{4C_{55j}i_1^2 I_{1j}}{5E_c L^4})\lambda^4 \tag{C-3}$$

$$L_{14} = 0 \tag{C-4}$$

$$L_{15} = -(\frac{h_m \pi I_{29e}}{h_e L})\lambda \tag{C-5}$$

$$L_{16} = -(\frac{\pi I_{29e}}{L})\lambda \tag{C-6}$$

$$L_{21} = (\frac{I_{5g}}{\rho_c h_c L})S^2 + (\frac{I_{15g}}{E_c h_c L})\lambda^2 + (\frac{\rho_e I_{9e}}{\rho_c h_c L})S^2 + (\frac{C_{11}I_{9e}}{E_c h_c L})\lambda^2 + (\frac{I_{9m}}{h_c L})S^2 + (\frac{I_{9m}}{h_c L})\lambda^2 + (\frac{4C_{55j}i_1^2 I_{9j}}{5E_c h_c L^3})\lambda^4$$
$$+(\frac{2C_{55j}i_0^2 I_{9j}}{E_c h_c L^3})\lambda^4 \tag{C-7}$$

$$L_{22} = (\frac{I_{5g}}{\rho_c h_c L^2})S^2 + (\frac{I_{17g}}{E_c h_c L^2})\lambda^2 + (\frac{k_s I_{21g}}{E_c h_c}) + (\frac{C_{11}I_{23e}}{E_c h_c L^2})\lambda^2 + (\frac{\rho_e I_{23e}}{\rho_c h_c L^2})S^2 + (\frac{C_{55e}k_s I_{23e}}{E_c h_c L^2}) + (\frac{I_{23e}}{h_c L^2})\lambda^2 + (\frac{I_{23m}}{h_c L^2})S^2$$
$$+(\frac{I_{23m}}{h_c L^2})\lambda^2 + (\frac{C_{55m}k_s I_{23m}}{E_c h_c L^2}) + (\frac{2C_{55j}i_0^2 I_{23j}}{E_c h_c L^3})\lambda^4 - (\frac{4C_{55j}i_1^2 I_{23j}}{5E_c h_c L^4})\lambda^4 + (\frac{C_{55j}i_2^2 I_{20j}}{8E_c h_c L^2})\lambda^2 + (\frac{24C_{55j}i_1^2 I_{20j}}{5E_c h_c L^2})\lambda^2 \tag{C-8}$$

$$L_{23} = (\frac{I_{7g}}{\rho_c h_c L^2})S^2 + (\frac{I_{13g}}{E_c h_c L^2})\lambda^2 + (\frac{k_s I_{18g}}{E_c h_c}) + (\frac{C_{11}I_{26e}}{E_c h_c L^2})\lambda^2 + (\frac{\rho_e I_{26e}}{\rho_c h_c L^2})S^2 + (\frac{C_{55e}k_s I_{11e}}{E_c h_c}) + (\frac{I_{26m}}{h_c L^2})\lambda^2 + (\frac{I_{26m}}{h_c L^2})S^2$$
$$+(\frac{C_{55m}k_s I_{11m}}{E_c h_c}) + 2(\frac{C_{55j}i_0^2 I_{26j}}{E_c h_c L^4})\lambda^4 + (\frac{4C_{55j}i_1^2 I_{26j}}{5E_c h_c L^4})\lambda^4 + (\frac{C_{55j}i_2^2 I_{11j}}{8E_c h_c L^2})\lambda^2 + (\frac{2C_{55j}i_0^2 I_{11j}}{E_c h_c L^2})\lambda^2 + (\frac{2C_{55j}i_0^2 I_{11j}}{E_c h_c L^2})\lambda^2 \tag{C-9}$$

$$L_{24} = (\frac{k_s I_{18e}}{E_c L})\lambda + (\frac{C_{55e}k_s I_{11e}}{E_c L})\lambda + (\frac{k_s I_{18m}}{E_c L})\lambda + (\frac{C_{55m}k_s I_{11}}{E_c L})\lambda - (\frac{C_{55j}i_2^2 I_{11j}}{8E_c L^3})\lambda^3 \tag{C-10}$$

$$L_{25} = -(\frac{\pi I_{33e}}{h_e L})\lambda - (\frac{e_{15} h_m I_{32e}}{h_e e_{31} L})\lambda \tag{C-11}$$

$$L_{26} = -(\frac{\pi I_{33m}}{h_m L})\lambda - (\frac{f_{15} I_{32m}}{f_{31} L})\lambda \tag{C-12}$$

$$L_{31} = (\frac{I_{4g}}{\rho_c h_c L})S^2 + (\frac{I_{14g}}{E_c h_c L^2})\lambda^2 + (\frac{I_{1e}}{h_c L})\lambda^2 + (\frac{I_{1e}}{h_c L})S^2 + (\frac{I_{1m}}{h_c L})\lambda^2 + (\frac{I_{1m}}{h_c L})S^2 + (\frac{4C_{55j}i_1^2 I_{1j}}{5E_c h_c L^3})\lambda^4 + (\frac{2C_{55j}i_0^2 I_{1j}}{E_c h_c L^3})\lambda^4 \qquad \text{(C-13)}$$

$$L_{32} = (\frac{I_{7g}}{\rho_c h_c L^2})S^2 - (\frac{I_{13g}}{E_c h_c L^2})\lambda^2 + (\frac{k_s I_{18e}}{E_c h_c}) + (\frac{C_{11}I_{26e}}{E_c h_c L})\lambda^2 + (\frac{\rho_e I_{26e}}{\rho_c h_c L^2})S^2 + (\frac{k_s C_{55e} I_{11e}}{E_c h_c}) + (\frac{I_{26m}}{h_c L})\lambda^2 \qquad \text{(C-14)}$$
$$+ (\frac{I_{26m}}{h_c L^2})S^2 + (\frac{k_s C_{55m} I_{11m}}{E_c h_c}) + (\frac{2C_{55j}i_0^2 I_{26j}}{E_c h_c L^3})\lambda^4 + (\frac{4C_{55j}i_1^2 I_{26j}}{5E_c h_c L^4})\lambda^4 + (\frac{4C_{55j}i_1^2 I_{11j}}{5E_c h_c L^2})\lambda^2 + (\frac{C_{55j}i_2^2 I_{11j}}{8E_c h_c L^2})\lambda^2$$
$$+ (\frac{2C_{55j}i_0^2 I_{11j}}{E_c h_c L^2})\lambda^2$$

$$L_{33} = (\frac{I_{6g}}{\rho_c h_c L^2})S^2 + (\frac{I_{16g}}{E_c h_c L^2})\lambda^2 + (\frac{k_s I_{12g}}{E_c h_c}) + (\frac{C_{11}I_{2e}}{E_c h_c L^2})\lambda^2 + (\frac{\rho_e I_{2e}}{\rho_c h_c L^2})S^2 + (\frac{k_s C_{55e} I_{0e}}{E_c h_c}) + (\frac{I_{2m}}{h_c L^2})\lambda^2 \qquad \text{(C-15)}$$
$$+ (\frac{I_{2m}}{h_c L^2})S^2 + (\frac{k_s C_{55m} I_{0m}}{E_c h_c}) + (\frac{4C_{55j}i_1^2 I_{2j}}{5E_c h_c L^4})\lambda^4 + (\frac{2C_{55j}i_0^2 I_{2j}}{E_c h_c L^4})\lambda^4 - (\frac{2C_{55j}i_0^2 I_{0j}}{E_c h_c L^2})\lambda^2 + (\frac{24C_{55j}i_1^2 I_{0j}}{5E_c h_c L^2})\lambda^2$$
$$+ (\frac{C_{55j}i_2^2 I_{0j}}{8E_c h_c L^2})\lambda^2$$

$$L_{34} = (\frac{k_s I_{12g}}{E_c L})\lambda + (\frac{k_s C_{55e} I_{0e}}{E_c L})\lambda + (\frac{k_s C_{55m} I_{0m}}{E_c L})\lambda - (\frac{1C_{55j}i_2^2 I_{0j}}{8E_c L^3})\lambda^3 + (\frac{16C_{55j}i_1^2 I_{0j}}{5E_c L^3})\lambda^3 \qquad \text{(C-16)}$$

$$L_{35} = -(\frac{e_{15} h_m I_{34e}}{h_m e_{31} L})\lambda - (\frac{\pi I_{30e}}{h_c L})\lambda \qquad \text{(C-17)}$$

$$L_{36} = -(\frac{f_{15} h_m I_{34m}}{h_m f_{31} L})\lambda - (\frac{\pi I_{30m}}{h_c L})\lambda \qquad \text{(C-18)}$$

$$L_{41} = 0 \qquad \text{(C-19)}$$

$$L_{42} = (\frac{k_s I_{18g}}{E_c L})\lambda + (\frac{k_s C_{55e} I_{11e}}{E_c L})\lambda + (\frac{k_s C_{55m} I_{11m}}{E_c L})\lambda - (\frac{1C_{55j}i_2^2 I_{11j}}{8E_c h_c L^3})\lambda^3 \qquad \text{(C-20)}$$

$$L_{43} = (\frac{k_s I_{12g}}{E_c L})\lambda + (\frac{k_s C_{55e} I_{0e}}{E_c L})\lambda + (\frac{k_s C_{55m} I_{0m}}{E_c L})\lambda - (\frac{C_{55j}i_2^2 I_{0j}}{8E_c L^3})\lambda^3 + (\frac{16C_{55j}i_1^2 I_{0j}}{5E_c L^3})\lambda^3 \qquad \text{(C-21)}$$

$$L_{44} = -(\frac{k_s h_s I_{12g}}{E_c L^2})\lambda^2 - (\frac{k_G h_c}{E_c L^2})\lambda^2 + (\frac{h_c I_{3g}}{\rho_c L^2})S^2 - (\frac{k_w h_c}{E_c}) + (\frac{N_e}{E_c h_c}) + (\frac{N_m}{E_c h_c}) - (\frac{h_c \rho_e I_{0e}}{\rho_c L^2})S^2 + (\frac{k_s h_c C_{55e} I_{0e}}{E_c L^2})\lambda^2 \qquad \text{(C-22)}$$
$$-(\frac{h_c I_{0m}}{L^2})S^2 + (\frac{k_s h_c C_{55m} I_{0m}}{E_c L^2})\lambda^2 + (\frac{32C_{55j}h_c i_1^2 I_{0j}}{15E_c L^4})\lambda^3 + (\frac{C_{55j}h_c i_2^2 I_{0j}}{8E_c L^4})\lambda^3$$

$$L_{45} = -(\frac{e_{15} h_m I_{34e}}{e_{31} L^2})\lambda^2 \qquad \text{(C-23)}$$

$$L_{46} = -\left(\frac{f_{15}\,h_m I_{34e}}{f_{31}L^2}\right)\lambda^2 \tag{C-24}$$

$$L_{51} = -\left(\frac{\pi I_{29m}}{h_c}\right)\lambda \tag{C-25}$$

$$L_{52} = -\left(\frac{e_{15}\,I_{32e}}{e_{31}L}\right)\lambda - \left(\frac{\pi I_{33m}}{h_c L}\right)\lambda \tag{C-26}$$

$$L_{53} = -\left(\frac{e_{15}\,I_{34e}}{e_{31}L}\right)\lambda - \left(\frac{\pi I_{30m}}{h_c L}\right)\lambda \tag{C-27}$$

$$L_{54} = -\left(\frac{e_{15}\,h_c I_{34e}}{e_{31}L^2}\right)\lambda^2 \tag{C-28}$$

$$L_{55} = -\left(\frac{h_{11}\,h_c E_c I_{27m}}{e_{31}^{\ 2}L^2}\right)\lambda^2 - \left(\frac{h_{33}\,\pi^2 E_c I_{28m}}{e_{31}^{\ 2}h}\right) \tag{C-29}$$

$$L_{56} = 0 \tag{C-30}$$

$$L_{61} = -\left(\frac{\pi I_{29m}}{h_c}\right)\lambda \tag{C-31}$$

$$L_{62} = -\left(\frac{f_{15}\,I_{32m}}{f_{31}L}\right)\lambda - \left(\frac{\pi I_{33m}}{h_c L}\right)\lambda \tag{C-32}$$

$$L_{63} = -\left(\frac{f_{15}\,I_{34m}}{f_{31}L}\right)\lambda - \left(\frac{\pi I_{30m}}{h_c L}\right)\lambda \tag{C-33}$$

$$L_{64} = -\left(\frac{f_{15}\,h_c I_{34m}}{f_{31}L^2}\right)\lambda^2 \tag{C-34}$$

$$L_{65} = 0 \tag{C-35}$$

$$L_{66} = -\left(\frac{\mu_{11}\,h_c E_c I_{27m}}{e_{31}^{\ 2}L^2}\right)\lambda^2 - \left(\frac{\mu_{33}\,\pi^2 E_c I_{28m}}{e_{31}^{\ 2}h}\right) \tag{C-36}$$

REFERENCES

[1] Salvetat, J. P., and A. Rubio. 2002. Mechanical properties of carbon nanotubes: a fiber digest for beginners. *Carbon* 40: 1729-1734.

[2] Esawi, A. M. K., and M. M. Farag. 2007. Carbon nanotube reinforced composites: potential and current challenges. *Material Design* 9: 2394-2401.

[3] Fiedler, B., F. H. Gojny, M. H. G. Wichmann, and et al. 2006. Fundamental aspects of nano-reinforced composites. *Composite Science and Technology:* 16: 3115-3125.

[4] Marynowski, K., 2018. vibration analysis of an axially moving sandwich beam with multiscale composite facings in thermal environment 146:116-124.

[5] Tao, Fu., T. Z. Chen, Yu. Hongying, Li. Chengfei, Z. Yanzheng. 2019. Thermal buckling and sound radiation behavior of truss core sandwich panel resting on elastic foundation. *International Journal of Mechanical Sciences* 161: 105055.

[6] Rafiee, M., He XQ. S, Mareishi, K. M. Liew. 2014. Modeling and stress analysis of smart CNTs/fiber/ polymer multiscale composite plates. *Int J Appl Mech* 6: 1450025.

[7] Li, Y. H., L. Wang, E. C. Yang. 2018. Nonlinear dynamic responses of an axially moving laminated beam subjected to both blast and thermal loads. *International Journal of Non-Linear Mechanics* 101: 56-67.

[8] Ansari, R., R. Gholami, S. Sahmani, A. Norouzzadeh, M. Bazdid-Vahdati. 2015. Dynamic Stability Analysis of Embedded Multi-Walled Carbon Nanotubes in Thermal Environment. *Acta Mechanica Solida Sinica* 28: 659-957.

[9] Kolahchi, R., M. Safari M. M. Esmailpour. 2015. Magneto-Thermo-Mechanical Buckling Analysis of Mindlin Plate Reinforced with FG-Carbon Nanotubes. *Archives of Civil Engineering* 62(3): 89-104.

[10] Lei, Y., M.I. Friswell, S. Adhikari. 2013. Vibration of nonlocal Kelvin-Voigt viscoelastic damped Timoshenko beams. *International Journal of Engineering Science* 66:1-13.

[11] Al-shujairi, M and Mollamahmutoglu C. 2018. investigated Buckling and free vibration analysis of functionally graded sandwich micro-beams resting on elastic foundation by using nonlocal strain gradient theory in conjunction with higher order shear theories under thermal effect, *Composites Part B.* 154:292-312.

[13] Mohammadimehr, M., B. Rousta Navi, A. Arani. 2016. Dynamic stability of modified strain gradient theory sinusoidal viscoelastic piezoelectric polymeric functionally graded single-walled carbon nanotubes reinforced nanocomposite plate considering surface stress and agglomeration effects under hydro-thermo-electro-magneto-mechanical loadings. *Mechanics of Advanced Materials and Structures*16: 1325-1342.

[14] Tagarielli, VL., VS. Deshpande, NA. Fleck. 2007. The dynamic response of composite sandwich beams to transverse impact. *International Journal of Solids and Structures* 44(7): 2442-2457.

[15] Tagarielli, VL., VS. Deshpande, NA. Fleck. 2010. Prediction of the dynamic response of composite sandwich beams under shock loading. *International Journal of Impact Engineering* 37(7): 854-864.

[16] Mohammadimehr, M., M. Emdadi, B. Rousta Navi. 2018. Dynamic stability analysis of micro composite annular sandwich plate with carbon nanotube reinforced composite facesheets based on modified strain gradient theory. *Journal of Sandwich Structures & Materials* 22: 1199-1234.

[17] Sahmani, S., and M. Bahrami. 2015. Size-dependent dynamic stability analysis of microbeams actuated by piezoelectric voltage based on strain gradient elasticity theory. *Journal of Mechanical Science and Technology* 29: 325-333.

[18] Loja, MAR. 2017. Dynamic response of soft core sandwich beams with metal-graphene nanocomposite skins. *Shock and Vibration*. Article ID 7842413: 16.

[19] Bhardwaj, G., A.K. Upadhyay, R Pandey, et al. 2012. Nonlinear flexural and dynamic response of CNT reinforced laminated composite plates. *Compos B* 45: 89–100.

[20] Talimian, A., and P. Beda. 2018. Dynamic stability of a size-dependent micro-beam. *European Journal of Mechanics / A Solids* 72: 245-251.

[21] Zamanzadeh, M., G. Rezazadeh, I. Jafarsadeghi poornaki. et al. 2013. Static and dynamic stability modeling of a capacitive FGM micro-beam in presence of temperature changes. *Applied Mathematical Modelling* 37: 6964-6978.

[22] Gao. K., W. Gao, D. Wu, et al. 2017. Nonlinear dynamic characteristics and stability of composite orthotropic plate on elastic foundation under thermal environment. *Composite Structures* 168: 619 -632.

[23] Songsuwan, W., M. Pimsarn, N. Wattanasakulpong. 2018. A study on dynamic response of functionally graded sandwich beams under different dynamic loadings. *MATEC Web of Conferences* 192: 02011.

[24] Ojha, RK., S.K. Dwivedy. 2020. Dynamic Analysis of a Three-Layered Sandwich Plate with Composite Layers and Leptadenia Pyrotechnica Rheological Elastomer-Based Viscoelastic Core. *Journal of Vibration Engineering & Technologies* 8: 541–553.

[25] Aguib, S., A. Nour, T. Djedid, et al. 2016. Forced transverse vibration of composite sandwich beam with magnetorheological elastomer core. *J Mech Sci Technol* 30: 15–24.

[26] Tessler, A., M. Di. Sciuva, M. Gherlone. 2009. A refined zigzag beam theory for composite and sandwich beams, *Journal of composite* 43(9):1051-1081.

[27] Ghorbanpour Arani, A., R. Kolahchi, H. Vossough. 2013. Buckling analysis and smart control of SLGS using elastically coupled PVDF nanoplate based on nonlocal Mindlin plate theory, *Physica B,* 407(22):4458-4465.

[28] Li, YS. 2014. Buckling analysis of magneto electro elastic plate resting on Pasternak elastic foundation. *Mech Res Commun* 56:104–114.

[29] Ebrahimi, F., and MR. Barati. 2016. Magnetic field effects on buckling behavior of smart size-dependent graded nanoscale beams. *Eur Phys J Plus* 131(7):238–251.

[30] Kerboua, M., A. Megnounif, M. Benguediab, and et al. 2015. Vibration control beam using piezoelectric-based smart materials, *Compos Structures* 123(5):430–442.

[31] Arefi M, Kiani M, Rabczuk T. Application of nonlocal strain gradient theory to size dependent bending analysis of a sandwich porous nanoplate integrated with piezomagnetic face-sheets. *Composites Part B: Engineering*. 2019 Jul 1;168:320-33.

[32] Arefi M, Zenkour AM. Size-dependent electro-elastic analysis of a sandwich microbeam based on higher-order sinusoidal shear deformation theory and strain gradient theory. *Journal of Intelligent Material Systems and Structures*. 2018 Apr;29(7):1394-406.

[33] Arefi M, Zenkour AM. Transient analysis of a three-layer microbeam subjected to electric potential. *International Journal of Smart and Nano Materials.* 2017 Jan 2;8(1):20-40.

[34] Arefi M, Allam MN. Nonlinear responses of an arbitrary FGP circular plate resting on the Winkler-Pasternak foundation. *Smart Struct. Syst.* 2015 Jul 1;16(1):81-100.

[35] Arefi M, Rabczuk T. A nonlocal higher order shear deformation theory for electro-elastic analysis of a piezoelectric doubly curved nano shell. *Composites Part B: Engineering.* 2019 Jul 1;168:496-510.

[36] Arefi M, Kiani M, Zenkour AM. Size-dependent free vibration analysis of a three-layered exponentially graded nano-/micro-plate with piezomagnetic face sheets resting on Pasternak's foundation via MCST. *Journal of Sandwich Structures & Materials.* 2020 Jan;22(1):55-86.

[37] Ke, LL., C. Liu, Y.S. Wang. 2015. Free vibration of nonlocal piezoelectric nanoplates under various boundary conditions, *Phys E* 66:93–106.

[38] Chen, D., J. Yang, S. Kitipornchai. 2015. Elastic buckling and static bending of shear deformable functionally graded porous beam. *Compos Structures* 133:54–61.

[39] Al Rjoub YS., A.G. Hamad .2017. Free vibration of functionally Euler-Bernoulli and Timoshenko graded porous beams using the transfer matrix method. *KSCE J Civ Eng* 21:792–806.

[40] Shafiei N., A. Mousavi, M. Ghadiri. 2016. On size-dependent nonlinear vibration of porous and imperfect functionally graded tapered microbeams. *Int J Eng Sci* 106:42–56.

[41] Chen D, S. Kitipornchai, J. Yang. 2016. Nonlinear free vibration of shear deformable sandwich beam with a functionally graded porous core. *Thin Walled Structures* 107:39–48.

[42] Saraswathy B., RR. Kumar, L. Mangal. 2012. Dynamic analysis of honeycomb sandwich beam with multiple debonds. *Mech Eng* 12:1-7.

[43] Navarro, P., S. Abrate, J. Aubry, and et al. 2013. Analytical modeling of indentation of composite sandwich beam. *Composite Structures* 100: 79–88.

[44] Girija Vallabhan, C.V., W. Thomas Straughan, Y.C. Das. 1991. Refined model for analysis of plates on elastic foundations. *J. Eng. Mech* 117(12): 2830–2843.

[45] Ghorbanpour Arani, A., and M. H. Zamani. 2018. Bending analysis of agglomerated carbon nanotube-reinforced beam resting on two parameters modified vlasov model foundation. *Indian Journal of Physics* 92: 767–777.

[46] Su, Z., G. J. Wang, Y. Wang, X. Ye. 2016. A general Fourier formulation for vibration analysis of functionally graded sandwich beams with arbitrary boundary condition and resting on elastic foundations. *Acta Mech* 227: 1493–1514.

[47] Ghorbanpour Arani, A., S. Amir. 2013. Electro-thermal vibration of visco-elastically coupled BNNT systems conveying fluid embedded on elastic foundation via strain gradient theory. *Physica B* 419:1–6.

[48] Arefi M, Bidgoli EM, Rabczuk T. Effect of various characteristics of graphene nanoplatelets on thermal buckling behavior of FGRC micro plate based on MCST. *European Journal of Mechanics-A/Solids.* 2019 Sep 1;77:103802.

[49] Arefi M, Bidgoli EM, Rabczuk T. Thermo-mechanical buckling behavior of FG GNP reinforced micro plate based on MSGT. *Thin-Walled Structures.* 2019 Sep 1;142:444-59.

[50] Arefi, M., A. M. Zenkour. 2017. Nonlocal electro-thermo-mechanical analysis of a sandwich nanoplate containing a Kelvin–Voigt viscoelastic nanoplate and two piezoelectric layers, *Acta Mech* 228: 475-493.

[51] Ghorbanpour Arani, A., M.H. Jalaei. 2016. Transient behavior of an orthotropic graphene sheet resting on orthotropic visco-Pasternak foundation. *International Journal of Engineering Science* 103: 97–113.

[52] Hajmohammad, M.H., M. Sharif Zarei, R. Kolahchi and et al. 2019. Visco-piezoelasticity zigzag theories for blast response of porous beams covered by grapheme platelet-reinforced piezoelectric layers. *Journal of Sandwich Structures & Materials* 0(0):1–27.